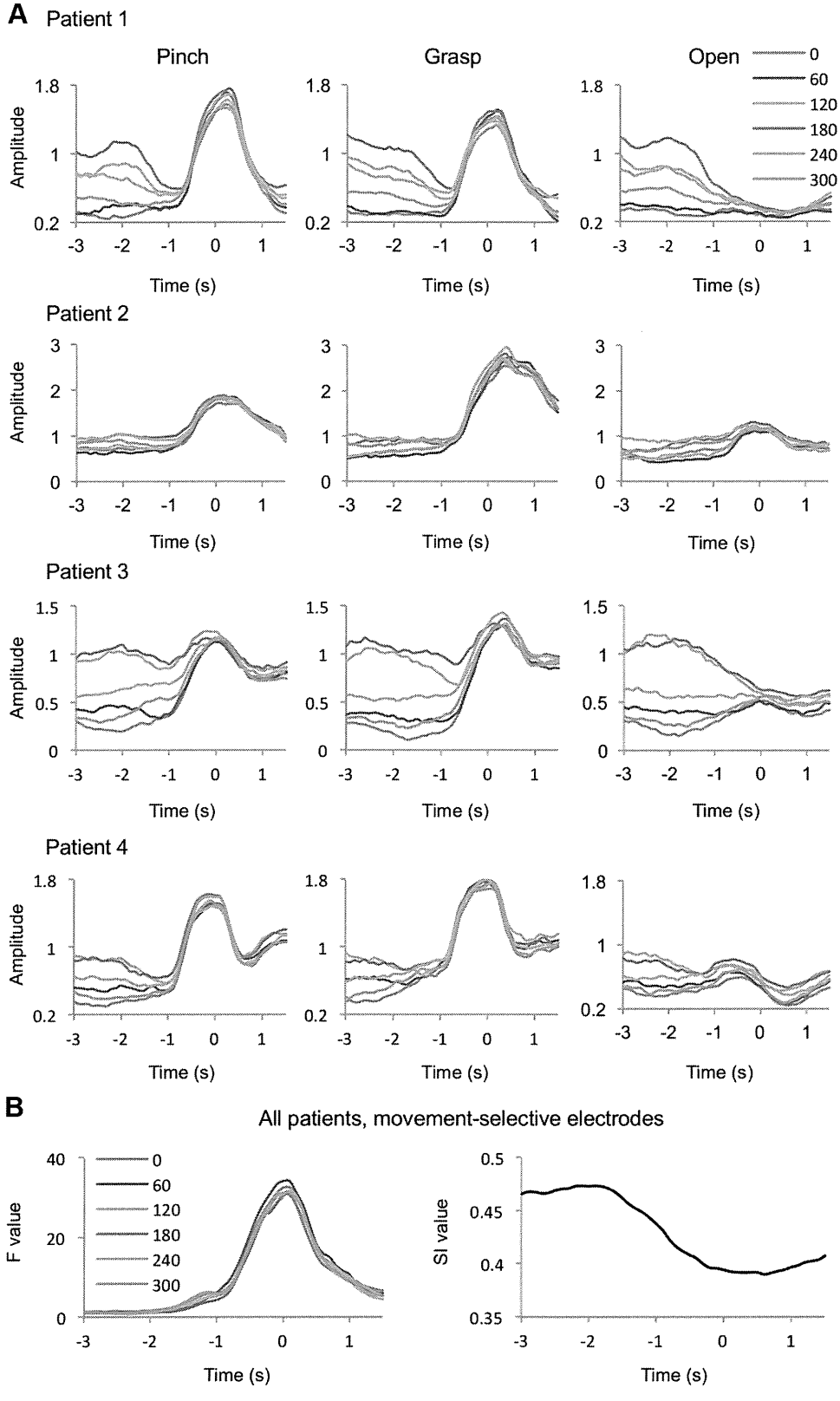

Figure 6. Hold-and-release regulation of the high-γ amplitude by PAC. ***A***, The mean α phase-conditioned high-γ amplitudes of each phase bin are shown for each movement type at the electrode with the highest *F* value for each patient. Each color corresponds to each α phase bin. ***B***, The mean *F* values (one-way ANOVA) for the α phase-conditioned high-γ amplitude among the movement types at the movement-selective electrodes of 4 patients are shown for each α phase bin (left). The time course of the mean SI value of the movement-selective electrodes of 4 patients is shown on the right.

2012). PAC may be used to select the cortical area that is relevant for movement classification. By selecting electrodes with strong PAC, the cortical area representing motor information could be effectively identified even before the execution of a movement. The selection of electrodes or regions based on PAC might help to reduce the number of model parameters, and thus improve the efficiency of model training. It may also be useful to compress signals for real-time transmission in brain-machine interface systems.

References

Axmacher N, Henseler MM, Jensen O, Weinreich I, Elger CE, Fell J (2010) Cross-frequency coupling supports multi-item working memory in the human hippocampus. Proc Natl Acad Sci U S A 107:3228–3233.

Bengio Y, Grandvalet Y (2004) No unbiased estimator of the variance of k-fold cross-validation. J Mach Learn Res 5:1089–1105.

Breiman L (1996) Heuristics of instability and stabilization in model selection. Ann Stat 24:2350–2383.

Bruns A, Eckhorn R (2004) Task-related coupling from high- to low-frequency signals among visual cortical areas in human subdural recordings. Int J Psychophysiol 51:97–116.

Canolty RT, Knight RT (2010) The functional role of cross-frequency coupling. Trends Cogn Sci 14:506–515.

Canolty RT, Edwards E, Dalal SS, Soltani M, Nagarajan SS, Kirsch HE, Berger MS, Barbaro NM, Knight RT (2006) High gamma power is phase-locked to theta oscillations in human neocortex. Science 313:1626–1628.

Cheyne D, Bells S, Ferrari P, Gaetz W, Bostan AC (2008) Self-paced movements induce high-frequency gamma oscillations in primary motor cortex. Neuroimage 42:332–342.

Churchland MM, Cunningham JP, Kaufman MT, Ryu SI, Shenoy KV (2010) Cortical preparatory activity: representation of movement or first cog in a dynamical machine? Neuron 68:387–400.

Cohen MX (2008) Assessing transient cross-frequency coupling in EEG data. J Neurosci Methods 168:494–499.

Cohen MX, Axmacher N, Lenartz D, Elger CE, Sturm V, Schlaepfer TE (2009) Nuclei accumbens phase synchrony predicts decision-making reversals following negative feedback. J Neurosci 29:7591–7598.

Crone NE, Miglioretti DL, Gordon B, Sieracki JM, Wilson MT, Uematsu S, Lesser RP (1998a) Functional mapping of human sensorimotor cortex with electrocorticographic spectral analysis. I. Alpha and beta event-related desynchronization. Brain 121:2271–2299.

Crone NE, Miglioretti DL, Gordon B, Lesser RP (1998b) Functional mapping of human sensorimotor cortex with electrocorticographic spectral analysis. II. Event-related synchronization in the gamma band. Brain 121:2301–2315.

Engel AK, Fries P (2010) Beta-band oscillations—signalling the status quo? Curr Opin Neurobiol 20:156–165.

Gilbertson T, Lalo E, Doyle L, Di Lazzaro V, Cioni B, Brown P (2005) Existing motor state is favored at the expense of new movement during 13–35 Hz oscillatory synchrony in the human corticospinal system. J Neurosci 25:7771–7779.

Gould IC, Rushworth MF, Nobre AC (2011) Indexing the graded allocation of visuospatial attention using anticipatory alpha oscillations. J Neurophysiol 105:1318–1326.

Haegens S, Händel BF, Jensen O (2011a) Top-down controlled alpha band activity in somatosensory areas determines behavioral performance in a discrimination task. J Neurosci 31:5197–5204.

Haegens S, Nácher V, Luna R, Romo R, Jensen O (2011b) α-Oscillations in the monkey sensorimotor network influence discrimination performance by rhythmical inhibition of neuronal spiking. Proc Natl Acad Sci U S A 108:19377–19382.

Händel B, Haarmeier T (2009) Cross-frequency coupling of brain oscillations indicates the success in visual motion discrimination. Neuroimage 45:1040–1046.

He BJ, Zempel JM, Snyder AZ, Raichle ME (2010) The temporal structures and functional significance of scale-free brain activity. Neuron 66:353–369.

Jensen O, Bonnefond M, VanRullen R (2012) An oscillatory mechanism for prioritizing salient unattended stimuli. Trends Cogn Sci 16:200–206.

Kamitani Y, Tong F (2005) Decoding the visual and subjective contents of the human brain. Nat Neurosci 8:679–685.

Klimesch W, Sauseng P, Hanslmayr S (2007) EEG alpha oscillations: the inhibition-timing hypothesis. Brain Res Rev 53:63–88.

Lakatos P, Karmos G, Mehta AD, Ulbert I, Schroeder CE (2008) Entrainment of neuronal oscillations as a mechanism of attentional selection. Science 320:110–113.

Luo H, Poeppel D (2007) Phase patterns of neuronal responses reliably discriminate speech in human auditory cortex. Neuron 54:1001–1010.

Mathewson KE, Lleras A, Beck DM, Fabiani M, Ro T, Gratton G (2011) Pulsed out of awareness: EEG alpha oscillations represent a pulsed-inhibition of ongoing cortical processing. Front Psychol 2:99.

Mazaheri A, Jensen O (2010) Rhythmic pulsing: linking ongoing brain activity with evoked responses. Front Hum Neurosci 4:177.

Miller KJ, Schalk G, Fetz EE, den Nijs M, Ojemann JG, Rao RP (2010) Cortical activity during motor execution, motor imagery, and imagery-based online feedback. Proc Natl Acad Sci U S A 107:4430–4435.

Mormann F, Fell J, Axmacher N, Weber B, Lehnertz K, Elger CE, Fernández G (2005) Phase/amplitude reset and theta-gamma interaction in the human medial temporal lobe during a continuous word recognition memory task. Hippocampus 15:890–900.

Muthukumaraswamy SD (2010) Functional properties of human primary motor cortex gamma oscillations. J Neurophysiol 104:2873–2885.

Neuper C, Pfurtscheller G (2001) Event-related dynamics of cortical rhythms: frequency-specific features and functional correlates. Int J Psychophysiol 43:41–58.

Osipova D, Hermes D, Jensen O (2008) Gamma power is phase-locked to posterior alpha activity. PLoS One 3:e3990.

Palva S, Palva JM (2007) New vistas for alpha-frequency band oscillations. Trends Neurosci 30:150–158.

Pineda JA (2005) The functional significance of mu rhythms: translating "seeing" and "hearing" into "doing." Brain Res Brain Res Rev 50:57–68.

Quian Quiroga R, Panzeri S (2009) Extracting information from neuronal populations: information theory and decoding approaches. Nat Rev Neurosci 10:173–185.

Ray S, Crone NE, Niebur E, Franaszczuk PJ, Hsiao SS (2008) Neural correlates of high-gamma oscillations (60–200 Hz) in macaque local field potentials and their potential implications in electrocorticography. J Neurosci 28:11526–11536.

Sabate M, Llanos C, Enriquez E, Rodriguez M (2012) Mu rhythm, visual processing and motor control. Clin Neurophysiol 123:550–557.

Sadaghiani S, Scheeringa R, Lehongre K, Morillon B, Giraud AL, Kleinschmidt A (2010) Intrinsic connectivity networks, alpha oscillations, and tonic alertness: a simultaneous electroencephalography/functional magnetic resonance imaging study. J Neurosci 30:10243–10250.

Saleh M, Reimer J, Penn R, Ojakangas CL, Hatsopoulos NG (2010) Fast and slow oscillations in human primary motor cortex predict oncoming behaviorally relevant cues. Neuron 65:461–471.

Sirota A, Montgomery S, Fujisawa S, Isomura Y, Zugaro M, Buzsáki G (2008) Entrainment of neocortical neurons and gamma oscillations by the hippocampal theta rhythm. Neuron 60:683–697.

Tamura Y, Hoshiyama M, Nakata H, Hiroe N, Inui K, Kaneoke Y, Inoue K, Kakigi R (2005) Functional relationship between human rolandic oscillations and motor cortical excitability: an MEG study. Eur J Neurosci 21:2555–2562.

Vanhatalo S, Palva JM, Holmes MD, Miller JW, Voipio J, Kaila K (2004) Infraslow oscillations modulate excitability and interictal epileptic activity in the human cortex during sleep. Proc Natl Acad Sci U S A 101:5053–5057.

Voytek B, Canolty RT, Shestyuk A, Crone NE, Parvizi J, Knight RT (2010) Shifts in gamma phase-amplitude coupling frequency from theta to alpha over posterior cortex during visual tasks. Front Hum Neurosci 4:191.

Yanagisawa T, Hirata M, Saitoh Y, Kato A, Shibuya D, Kamitani Y, Yoshimine T (2009) Neural decoding using gyral and intrasulcal electrocorticograms. Neuroimage 45:1099–1106.

Yanagisawa T, Hirata M, Saitoh Y, Goto T, Kishima H, Fukuma R, Yokoi H, Kamitani Y, Yoshimine T (2011) Real-time control of a prosthetic hand using human electrocorticography signals. J Neurosurg 114:1715–1722.

Yanagisawa T, Hirata M, Saitoh Y, Kishima H, Matsushita K, Goto T, Fukuma R, Yokoi H, Kamitani Y, Yoshimine T (2012) Electrocorticographic control of a prosthetic arm in paralyzed patients. Ann Neurol 71:353–361.

Epilepsy Research (2013) **103**, 195—204

journal homepage: www.elsevier.com/locate/epilepsyres

Altered extrafocal iomazenil activity in mesial temporal lobe epilepsy

Koichi Hosomi[a,b], Haruhiko Kishima[a,*], Satoru Oshino[a], Masayuki Hirata[a], Naoki Tani[a,c], Tomoyuki Maruo[a], Hui Ming Khoo[a], Eku Shimosegawa[d], Jun Hatazawa[d], Amami Kato[e], Toshiki Yoshimine[a]

[a] *Department of Neurosurgery, Osaka University Graduate School of Medicine, Osaka, Japan*
[b] *Department of Neuromodulation and Neurosurgery, Office for University-Industry Collaboration, Osaka University, Osaka, Japan*
[c] *Department of Neurosurgery, Otemae Hospital, Osaka, Japan*
[d] *Department of Nuclear Medicine and Tracer Kinetics, Osaka University Graduate School of Medicine, Osaka, Japan*
[e] *Department of Neurosurgery, Kinki University Faculty of Medicine, Osaka, Japan*

Received 7 February 2012; received in revised form 6 June 2012; accepted 3 July 2012
Available online 20 July 2012

KEYWORDS
Iomazenil SPECT;
Interhemispheric asymmetry;
Mesial temporal lobe epilepsy;
Central benzodiazepine receptor

Summary To investigate involvement of extrafocal regions in mesial temporal lobe epilepsy (MTLE), we retrospectively explored abnormalities in distribution of iomazenil (IMZ) activity by identifying interhemispheric asymmetry on IMZ-SPECT images of patients with MTLE. Fourteen MTLE patients in whom a good surgical outcome was achieved were included in the study. Voxel-based (VB) analysis and volume-of-interest (VOI) analysis with predefined VOIs were applied to compare IMZ binding between the hemispheres ipsilateral and contralateral to the epileptic focus. VB analysis showed significant decreases in iomazenil binding not only in the ipsilateral anterior temporal lobe including the mesial temporal structures but also in the ipsilateral extratemporal region including the insula, putamen, and medial occipital lobe. VOI analysis showed similar significant decreases in the ipsilateral parahippocampal gyrus, amygdala, putamen, lateral temporal lobe, and lateral occipital lobe. Results of the SPECT analyses suggest that decreased or dysfunctional IMZ activity extends from the mesial temporal lobe to the ipsilateral extrafocal region in patients with MTLE.

Introduction

Mesial temporal lobe epilepsy (MTLE) is one of the main types of partial-onset epilepsy and is characterized by seizures that originate in the hippocampus, amygdala, or other mesial structures in the temporal lobe. Several studies have shown that the histologic, morphologic, and functional brain abnormalities associated with MTLE extend

* Corresponding author at: Department of Neurosurgery, Osaka University Graduate School of Medicine, 2-2 Yamadaoka, Suita, Osaka 565-0871, Japan. Tel.: +81 6 6879 3652; fax: +81 6 6879 3659.
E-mail address: hkishima@nsurg.med.osaka-u.ac.jp (H. Kishima).

0920-1211/$ — see front matter © 2012 Elsevier B.V. All rights reserved.
http://dx.doi.org/10.1016/j.eplepsyres.2012.07.001

beyond the mesial temporal lobe to regions adjacent to the hippocampus as well as extratemporal structures (Henry et al., 1990; Arnold et al., 1996; Dupont et al., 1998; Hammers et al., 2001; Bouilleret et al., 2002; Cendes et al., 2005; Didelot et al., 2010). These abnormalities have been evaluated in resected specimens, at autopsy, by magnetic resonance imaging (MRI), and by nuclear imaging.

Central benzodiazepine receptor (cBZR) labeling is used in nuclear imaging to identify epileptic foci. Expression of cBZR, a component of the gamma-aminobutyric acid (GABA)-A receptor complex, can represent inhibitory function of the brain (Umeoka et al., 2007). A histological study of brain tissues obtained from animal epilepsy models revealed decreased cBZR density in the epileptic foci (Kurokawa et al., 1994). Examination of slice preparations of human brain tissues taken from epileptic foci also revealed decreased cBZR density (Johnson et al., 1992).

^{11}C-flumazenil (FMZ) is a selective cBZR antagonist used as a positron emission tomography (PET) tracer, and ^{123}I-iomazenil (IMZ) is a selective cBZR agonist used in single photon emission computed tomography (SPECT); both have been used to detect epileptic foci. IMZ-SPECT has come into widespread use for presurgical detection of epileptic foci (Kaneko et al., 2006; Umeoka et al., 2007) because of the availability of both tracer and gamma camera. However, few IMZ-SPECT studies have examined extrafocal alterations in the whole brain of patients with MTLE, except for studies examining the diagnostic value of IMZ-SPECT (Tanaka et al., 1997; Kaneko et al., 2006; Umeoka et al., 2007). We conducted a retrospective study of IMZ-SPECT images to explore abnormalities, i.e., interhemispheric asymmetry, in IMZ activity in patients with MTLE. We used two different analytical methods: voxel-based (VB) analysis with statistical parametric mapping (SPM) and predefined volume-of-interest (VOI) analysis with three-dimensional stereotactic surface projection (3D-SSP). Both methods are excellent in terms of reproducibility and objectivity, owing to automatic spatial normalization and statistical analysis of the whole brain (Minoshima et al., 1994; Friston et al., 1995a,b; Minoshima et al., 1995; Hosoda et al., 2005; Takada et al., 2006).

Methods

Patients

Fourteen patients with refractory MTLE who were treated surgically at our hospital between 2004 and 2010 and in whom a satisfactory surgical outcome, i.e., Engel's class I or II (Engel et al., 1993), was achieved were included in the study (11 females, 3 males; median age at seizure onset: 7.5 years, range: 1–24 years; median age at surgery: 19 years, range: 13–46 years; median follow-up time after surgery: 57 months, range: 12–85 months). All 14 patients had undergone preoperative interictal IMZ-SPECT at our hospital while receiving antiepileptic medications. All antiepileptic medications, including benzodiazepines (clonazepam, 2–6 mg daily; clobazam, 10–30 mg daily), were continued. Clinical characteristics of the 14 patients are summarized in Table 1.

The preoperative diagnoses of MTLE were based on clinical history, semiology, and MRI, interictal ^{18}F-fluorodeoxyglucose (FDG) PET, magnetoencephalographic monitoring, and long-term video scalp electroencephalography (EEG) findings. All patients suffered daily to monthly seizures despite appropriate medical treatment with several antiepileptic drugs for more than 1 year after seizure onset. Most patients showed typical MTLE semiology, i.e., abdominal aura ($n = 12$), automatism ($n = 10$), dystonic posturing ($n = 4$). Brain MRI revealed ipsilateral hippocampal atrophy in 10 patients and signal intensity changes in the ipsilateral hippocampus on T2-weighted and/or FLAIR images in 9 of these 10 patients. MRI revealed a parahippocampal lesion in one patient (Patient 1). No MRI abnormalities were seen in the remaining three patients.

All surgeries had been comprehensively planned on the basis of preoperative examinations with ($n = 6$) or without ($n = 8$) invasive EEG recordings and were guided by intraoperative electrocorticography. Selective amygdalohippocampectomy was performed in 13 patients. Outcomes more than 1 year after surgery were regarded corresponding to Engel's class I (Engel et al., 1993), except in one case. Histopathologic examination of resected tissues revealed hippocampal sclerosis ($n = 10$), cortical dysplasia of the parahippocampal gyrus ($n = 2$), gliosis ($n = 1$), and ganglioglioma ($n = 1$), confirming that the epileptic foci were located in mesial temporal structures and that the diagnosis of MTLE was accurate in all cases.

Acquisition of SPECT images

IMZ-SPECT had been performed in all 14 patients in the interictal state; all were taking antiepileptic medications. Delayed images, which reflect mainly tracer binding to cBZR (Beer et al., 1990; Schubiger et al., 1991; Tanaka et al., 1997), were acquired 3 h after intravenous injection of 167 MBq ^{123}I-IMZ. A four-headed gamma camera (Gamma View SPECT 2000H, Hitachi, Tokyo, Japan) equipped with low-energy middle-resolution parallel-hole collimators (64 × 64 matrix) was used (intrinsic spatial resolution, 3.1 mm full width at half maximum, useful field of view) (Kimura et al., 1990). Raw data were obtained at 20 s per step over a 360° rotation. Transaxial images (voxel size, 4 mm × 4 mm × 4 mm) were reconstructed with a Butterworth filter (cut-off frequency 0.20 cycle/pixel, order 10) and attenuation correction (Chang method, attenuation coefficient: 0.08/cm). Qualitative images were created, and the hemispheres ipsilateral and contralateral to the epileptic focus were compared.

VB analysis of IMZ-SPECT images

Because the epileptic focus was left-sided in six patients and right-sided in eight patients, the IMZ-SPECT images obtained from the six patients with left MTLE were left-right flipped before preprocessing (MRIcro; http://www.sph.sc.edu/comd/rorden/mricro.html) to align the epileptogenic zone on the right side, as previously described (Kim et al., 2003; Hammers et al., 2008). These alignments let all 14 cases be statistically analyzed together.

Table 1 Patients' clinical characteristics.

Patient	Age (y)	Sex	Age at seizure onset (y)	Seizures	Medication (s)	Laterality	MRI findings	Histology	Scalp EEG	IMZ-SPECT: decreases	FDG-PET: decreases	Invasive EEG	Outcome[a]
1	14	F	1	Weekly SPS and CPS	CBZ, CLB, CZP	Rt	Lesion (Rt PHG)	Ganglioglioma	Rt T (interictal) SP2 (ictal)	Rt m-T	Rt m-T	–	Ia
2	30	F	8	Weekly SPS, Monthly CPS	CBZ, CLB, CZP	Rt	Rt HA, HI	HS	Rt FT (interictal)	–	Rt m-T	Rt m-T (ictal)	Ia
3	28	F	19	Monthly CPS	CBZ	Lt	Lt HA, HI	HS	F3, T3 (interictal) Lt (ictal)	Lt T	Lt T	Lt tip-m-T (ictal)	Ia
4	21	M	4	Daily SPS, Monthly CPS and SGS	PHT, VPA	Rt	–	HS	Rt T (interictal)	Rt T	Rt m-T	–	Ia
5	13	F	10	Daily SPS, Weekly CPS	CBZ	Rt	–	CD	Rt FT (interictal) Rt FT (ictal)	Rt TP, Lt m-T	Rt T, Rt F, Rt O	Rt m-T (ictal)	Ia
6	14	F	11	Weekly SPS and CPS	VPA, ZNS, CLB	Lt	Lt HA, HI	HS	Lt T (interictal) Lt T (ictal)	Lt m-tip-T, Bil m-F	Bil base-T, Bil Thal	–	Ia
7	46	M	24	Monthly SPS	PHT, PB	Rt	–	Gliosis	SP2 (interictal)	Bil T	Rt m-T, Rt l-T	–	Ia
8	19	F	1	Weekly SPS and CPS	ZNS, CZP	Lt	Lt HA, HI	CD	Bil F-C, Lt T (interictal) Lt T (ictal)	Lt m-base-T, Bil F	Lt m-T	Lt m-T (ictal)	IIa
9	17	F	10	Daily CPS	PHT, ZNS, AZA	Lt	Lt HA, HI	HS	Lt FT (ictal)	Lt m-tip-T	Lt m-tip-l-T	–	Ia
10	16	F	2	Weekly CPS, Yearly SGS	VPA, TPM	Lt	Lt HA, HI	HS	T3, SP1 (ictal)	Lt m-T, Lt l-T	Lt m-T	–	Ia
11	33	F	3	Dialy SPS, Monthly CPS	CLB	Rt	Rt HA, HI	HS	F8 (interictal)	Rt m-T	Rt m-T, Rt l-T	–	Ib
12	22	F	7	Weekly CPS	VPA, LTG	Rt	Rt HA, HI	HS	F8, T4, SP2 (interictal) T4 (ictal)	Rt m-T	Rt m-tip-T	Rt base-T (interictal)	Ia
13	16	M	3	Daily CPS, Monthly SGS	LTG, PHT, TPM, ZNS	Lt	Lt HA	HS	F7 (interictal) F7 (ictal)	Lt l-T	Lt m-tip-T	Lt m-T (ictal)	Ia
14	19	F	12	Monthly CPS	CBZ, CLB	Rt	Rt HA, HI	HS	F4 (interictal) Rt FT (ictal)	Rt m-T, Rt l-T	Rt T	–	Ia

y, year; m, month; F, female; M, male; SPS, simple partial seizure; CPS, complex partial seizure; SGS, secondary generalized seizure; CBZ, carbamazepine; CLB, clobazam; CZP, clonazepam; PHT, phenytoin; VPA, valproate; ZNS, zonisamide; PB, phenobarbital; AZA, acetazolamide; TPM, topiramate; LTG, lamotrigine; Lt, left; Rt, right; Bil, bilateral; HA, hippocampal atrophy; HI, hippocampal high signal intensity on T2-weighted and/or FLAIR images; PHG, parahippocampal gyrus; HS, hippocampal sclerosis; CD, cortical dysplasia; T, temporal lobe; SP, sphenoidal electrode; FT, fronto-temporal lobe; TP, temporo-parietal lobe; F, frontal lobe; O, occipital lobe; Thal, thalamus; m-, medial part; base-, basal part; l-, lateral part.

[a] Reported as Engel's classification (Engel et al., 1993).

Spatial preprocessing and statistical analysis of SPECT images were performed with SPM8 (Wellcome Department of Imaging Neuroscience, Institute of Neurology, University College London, London, UK) implemented in MATLAB 7.11.0 (MathWorks Inc., Massachusetts, USA) (Friston et al., 1995a,b; Kugaya et al., 2003; Heinzel et al., 2008). SPM8 provides for statistical parametric mapping of neuroimaging data. Individual SPECT images were spatially normalized to the standard stereotactic space (voxel size, 2 mm × 2 mm × 2 mm) of the Montreal Neurological Institute (MNI) brain by applying a symmetrical SPECT template created from an asymmetrical template provided in SPM8 (Didelot et al., 2010). This spatial normalization was performed by using the optimum 12-parameter affine transformation and nonlinear deformations. The accuracy of spatial normalization was visually confirmed on the display by comparing the normalized images to the template. The normalized images were smoothed with a 12-mm FWHM Gaussian filter to increase the signal-to-noise ratio. Global nuisance effects were removed by including the global covariate as a nuisance effect in the general linear model (ANCOVA). Interhemispheric asymmetry was examined in all 14 patients with right or ''flipped right'' MTLE to detect relative decrease and increase in IMZ binding. IMZ binding in the ipsilateral (right) hemisphere was compared (voxel-by-voxel) to that in the contralateral (left) hemisphere, and the difference was analyzed by paired t test with SPM8. Differences in uncorrected voxel levels were considered significant at $p < 0.001$, and those in uncorrected cluster levels were considered significant at $p < 0.05$. One hundred or more contiguous voxels were examined in the ipsilateral (right) hemisphere, including the epileptic focus (Van Bogaert et al., 2000; Kim et al., 2003). Coordinates of interest were converted from MNI space to the Talairach atlas by using the Brett transform (Brett et al., 2002), and areas of interest were localized according to the Talairach atlas (Talairach and Tournoux, 1988).

VOI analysis of IMZ-SPECT images

The automatic VOI analysis toolkit (VOIClassic) included in NEUROSTAT software library (Nihon Medi-Physics Co. Ltd., Tokyo, Japan) was applied to evaluate asymmetry of IMZ binding in each VOI (Hosoda et al., 2005; Takada et al., 2006). The program automatically calculated the average count per voxel in a VOI, which was predefined on the standard stereotactic space of the Talairach atlas covering the whole brain. Each original SPECT image was first stereotactically transformed into a standard 3D surface image by making use of the 3D-SSP in NEUROSTAT (Minoshima et al., 1994, 1995; Ishii et al., 2001). The original images were spatially normalized to the standard stereotactic space according to the Talairach atlas by applying the IMZ-SPECT template provided in NEUROSTAT, and the peak cortical activity within six voxels from the brain surface was projected onto the surface voxels. After accuracy of the spatial normalization was checked, VOIClassic calculated the average count in each of the 37 predefined VOIs on the transformed surface images. The predefined 37 VOIs were provided by VOIClassic software and consisted of the bilateral VOIs listed in Table 3, pons, whole cerebral cortices, and whole brain. For each individual, each average count was divided by the individual total count of the whole cerebellum to correct for global inter-individual differences. The corrected counts of all 14 patients were then compared between the ipsilateral and contralateral sides in each region by paired t test. Values are shown as mean corrected counts ± SD. Differences were considered significant at $p < 0.05$.

Table 2 Areas of significantly decreased iomazenil binding (according to voxel-based analysis).

Area	Peak	Cluster		Talairach coordinates of peaks (x, y, z, mm)/voxel equivalent Z		
		p value	Size (voxels)			
Anterior temporal, Insula, Putamen, Supratemporal		< 0.001	5189			
	Temporal tip (STG, BA38)			45, 10, −28/6.14		(A)
	Medial temporal (Hippocampus, BA28)			20, −13, −15/5.06		(B)
	Lateral temporal (MTG, BA21)			41, −1, −25/4.90		(C)
	Temporal stem			27, 16, −12/4.75	40, 10, −10/4.40	(D)
	Temporal tip (BA36)			36, 2, −36/4.71	27, −3, −34/4.56	(E)
	Insula, Putamen			33, −23, 15/3.86		(F)
	Lateral temporal (STG, BA22)			56, −5, 1/3.73		(G)
	Medial supratemporal plane			43, −30, 16/3.67		(H)
Medial occipital	(Cuneus, BA18)	0.006	173	3, −77, 10/3.95		(I)

STG, superior temporal gyrus; BA, Brodmann's area; MTG, middle temporal gyrus.

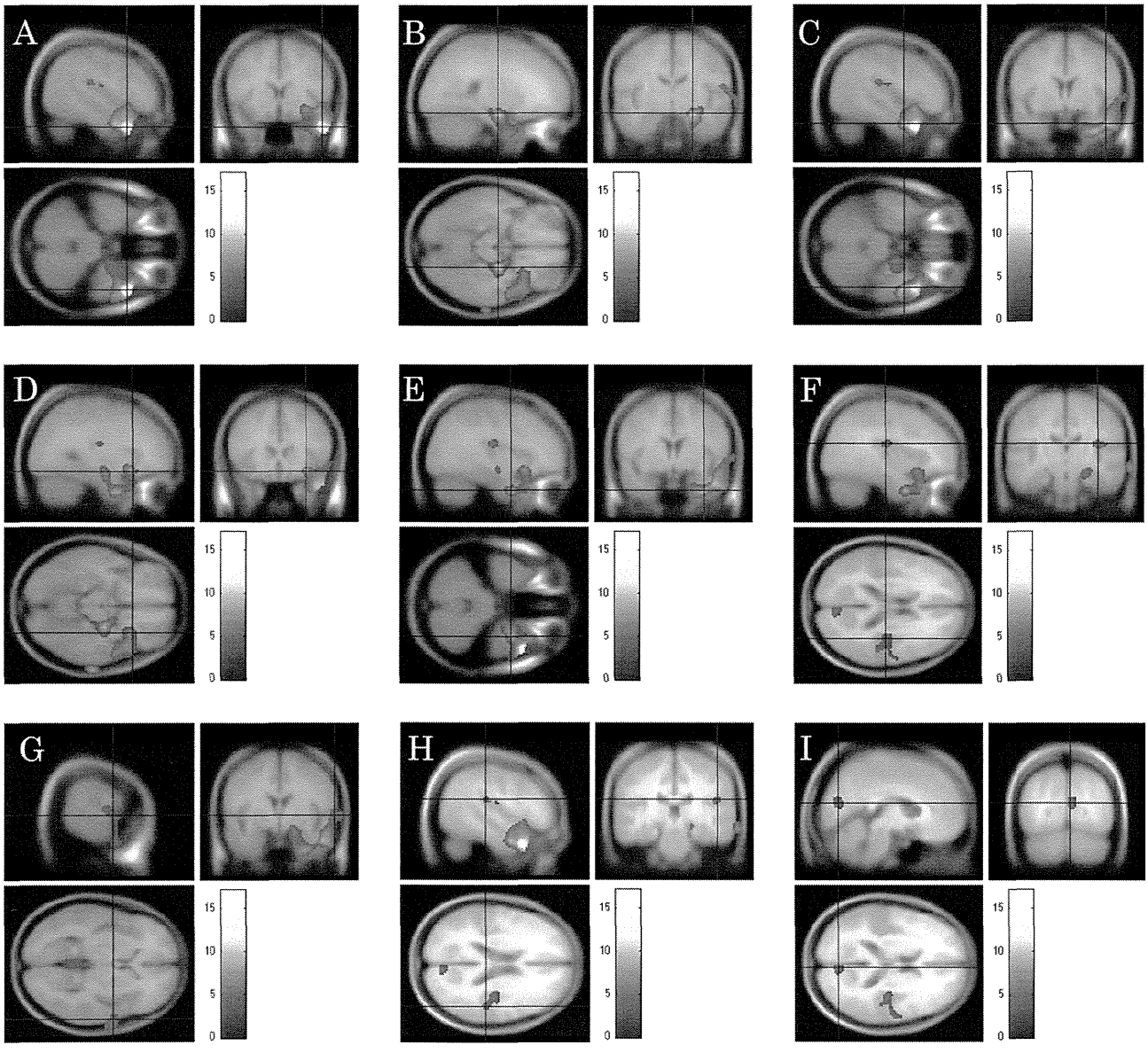

Figure 1 Statistical parametric maps (Z maps) of intensity on normalized images obtained from all 14 patients. Significant decreases in IMZ binding in the hemisphere ipsilateral to the epileptic focus were present in the anterior temporal lobe (A–E, G), the insula, putamen, and supratemporal plane (F, H), and the medial occipital lobe (I). Color bars show the *Z* score scale. Panels A–K correspond to Table 2.

Results

VB analysis of the IMZ-SPECT images from all 14 patients revealed significantly decreased IMZ binding in the following areas of the hemisphere ipsilateral to the epileptic focus: the anterior temporal lobe, insula, putamen, and supratemporal plane (cluster size, 5189 voxels; $p < 0.001$); and the medial occipital lobe (cluster size, 173 voxels; $p = 0.006$). Decreases in the anterior temporal lobe included decreases in the medial, tip, and lateral parts, including the hippocampus. Significant increases in IMZ binding were not seen in the ipsilateral hemisphere (Table 2, Fig. 1).

VOI analysis of the IMZ-SPECT images from all 14 patients revealed significantly decreased IMZ binding in the parahippocampal gyrus and amygdala on the ipsilateral side vs. the contralateral side: 0.620 ± 0.106 vs. 0.714 ± 0.061, $p = 0.004$; 0.660 ± 0.118 vs. 0.762 ± 0.092, $p < 0.001$. Counts were also significantly lower on the ipsilateral side (vs. contralateral side) in the putamen, lateral temporal lobe, and lateral occipital lobe: 0.618 ± 0.108 vs. 0.696 ± 0.146, $p = 0.012$; 1.270 ± 0.084 vs. 1.301 ± 0.083, $p = 0.023$; 1.475 ± 0.108 vs. 1.518 ± 0.137, $p = 0.005$. There were no ipsilateral VOIs with significantly higher counts (Table 3, Fig. 2).

Discussion

This study is the first to document altered IMZ activity in the anterior temporal and extratemporal regions in MTLE

Table 3 Corrected iomazenil counts within each VOI.

VOI	Mean (SD)		*p* value*
	Ipsilateral side	Contralateral side	
Lateral frontal cortex	1.302 (0.099)	1.308 (0.102)	0.475
Lateral temporal cortex	1.270 (0.084)	1.301 (0.083)	0.023*
Lateral parietal cortex	1.411 (0.114)	1.416 (0.110)	0.633
Lateral occipital lobe	1.475 (0.108)	1.518 (0.137)	0.005*
Anterior cingulate cortex	0.932 (0.123)	0.937 (0.122)	0.487
Posterior cingulate cortex	1.131 (0.141)	1.114 (0.128)	0.187
Medial frontal cortex	1.229 (0.106)	1.245 (0.096)	0.195
Medial parietal cortex	1.436 (0.111)	1.407 (0.119)	0.139
Primary sensorimotor cortex	1.365 (0.102)	1.385 (0.119)	0.130
Primary visual cortex	1.851 (0.161)	1.863 (0.167)	0.564
Caudate nucleus	0.469 (0.089)	0.474 (0.090)	0.655
Cerebellar hemisphere	0.936 (0.036)	0.939 (0.033)	0.728
Cerebellar vermis	1.170 (0.099)	1.180 (0.087)	0.561
Putamen	0.618 (0.108)	0.696 (0.146)	0.012*
Parahippocampal gyrus	0.620 (0.106)	0.714 (0.061)	0.004*
Amygdala	0.660 (0.118)	0.762 (0.092)	<0.001*
Thalamus	0.344 (0.074)	0.338 (0.101)	0.706

VOI, volume of interest predefined on the standard stereotactic space of the Talairach atlas. Sides are ipsilateral and contralateral to the epileptic focus.

* For difference in mean count between the ipsilateral and contralateral sides.

patients by means of IMZ-SPECT. Interhemispheric comparison revealed significant decreases in IMZ activity in the hemisphere ipsilateral to the epileptic focus, not only in the anterior and mesial temporal lobe but also in extratemporal regions.

To analyze altered IMZ activity in MTLE patients, we investigated asymmetry of IMZ uptake between hemispheres ipsilateral and contralateral to the epileptic focus. Two different methods, VB analysis with SPM and VOI analysis with 3D-SSP, were applied. VB analysis automatically shows areas of statistical significance in the whole brain. VOI analysis by 3D-SSP with predefined VOIs is also fully automatic. Manual delineation of regions of interest (ROIs) is widely used in comparative imaging. However, it is difficult to place ROIs manually on SPECT images because of the low spatial resolution. Thus, we used two more objective methods, VB and VOI analyses, in this study.

For our multi-subject analyses, brains were normalized into a standard brain space. VB statistical analysis with SPM can analyze the whole brain exhaustively and can evaluate the detailed extent of abnormalities on a voxel or cluster level. Such statistical voxel-based analysis was established by Friston et al. (1995a,b) and later applied in many studies. The VOI analysis uses a predefined set of VOIs on the standard stereotactic space of the Talairach atlas to eliminate rater-dependent bias (Hosoda et al., 2005; Takada et al., 2006). Spatial normalization with 3D-SSP, which was applied before calculation of the average counts in VOIs, has a particular advantage in the atrophic brain (Ishii et al., 2001).

The VB and VOI data represented intra-individual differences and relative interhemispheric asymmetry. Interhemispheric asymmetry analysis has been widely applied in both research and clinical settings (Kim et al., 2003; Aubert-Broche et al., 2005; Hammers et al., 2008; Didelot et al., 2010). Interhemispheric asymmetry analysis of FDG-PET images correctly detected the epileptic zone in 69% of patients in whom simple comparisons revealed no significant or bilateral temporal hypometabolism (Kim et al., 2003); this analysis was also thought to reduce the false-positive findings and correctly identify true-positive findings (Hammers et al., 2008). Moreover, these methods can be applied without a normal control group, can evaluate regions of low IMZ activity, and may be acceptable for analysis with qualitative images. Six of our 14 patients were taking benzodiazepines, which can partially block binding of IMZ. The interhemispheric asymmetry analysis makes results interpretable in such cases. In line with these reported applications, we analyzed interhemispheric asymmetry of IMZ uptake in our patients.

To analyze all data from all 14 of our patients together, the IMZ-SPECT images obtained from the 6 patients with left MTLE were left-right flipped, as previously reported (Kim et al., 2003; Hammers et al., 2008). The side of the epileptic focus and the exact histologic diagnosis were confirmed in each patient on the basis of the post-surgical outcomes.

The late IMZ-SPECT images are thought to correspond to retention of the tracer at specific cBZR binding sites, and the early images are thought to depict both regional CBF and cBZR density (Beer et al., 1990; Schubiger et al., 1991; Tanaka et al., 1997). When we use FMZ-PET, measuring the arterial input function is important to accurately determine cBZR density with adequate exclusion of the regional variations in cerebral blood flow (CBF) (Hammers et al., 2008). Because of the long half-life of IMZ tracer, we can easily obtain late Images 3 h after injection. Therefore, we relied on the late images reflecting cBZR density without measuring arterial input function.

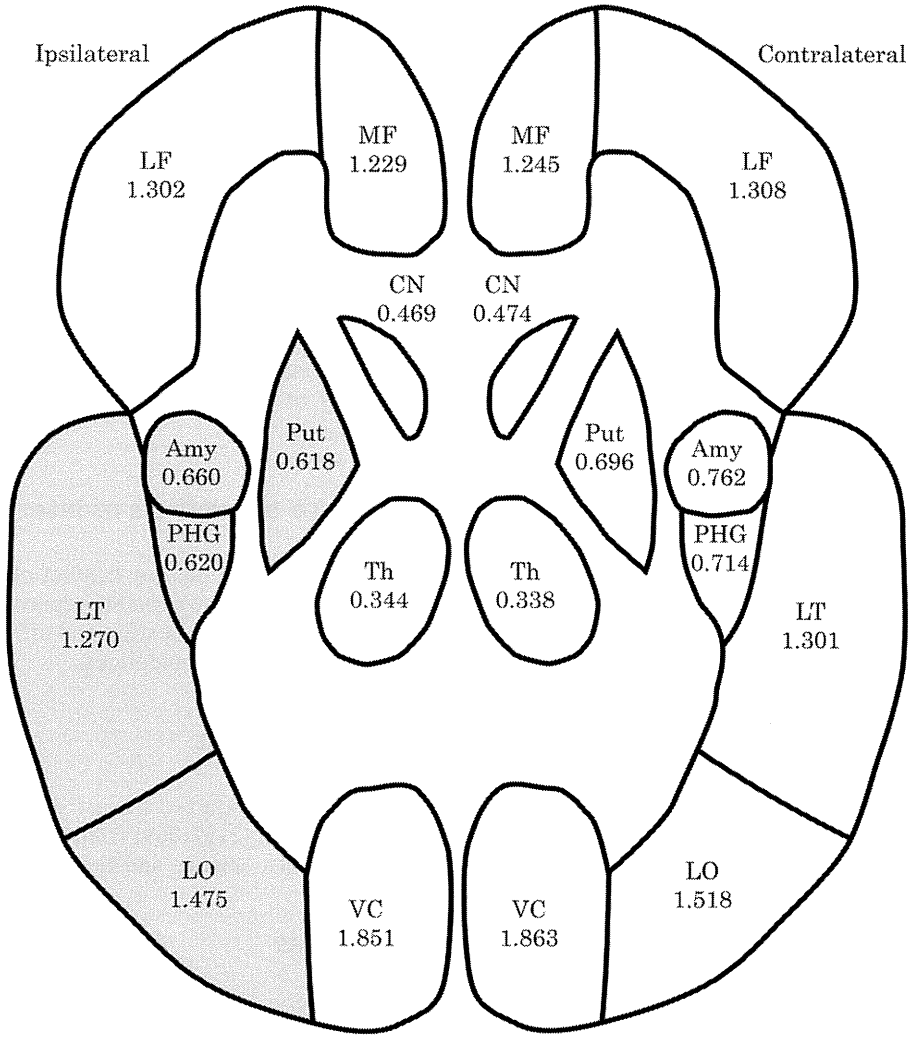

Figure 2 Schematic drawing of the topography of each average count. The ipsilateral gray regions have significantly lower counts than those on the contralateral side. Each mean corrected count is shown for each region. LF, lateral frontal lobe; MF, medial frontal lobe; LT, lateral temporal lobe; LO, lateral occipital lobe; VC, primary visual cortex; Amy, amygdala; PHG, parahippocampal gyrus; CN, caudate nucleus; Put, putamen; Th, thalamus.

We performed only group analysis in this study. If a normal control set or thresholds of normal asymmetry become available, further individual analysis could be performed. Such analysis might be useful for clinical diagnosis in individual patients and pathophysiologic consideration of individual symptoms.

Abnormalities in the temporal lobe

VB analysis showed that the most significant decreases in IMZ binding extended widely from the medial part to the temporal tip and lateral part of the anterior temporal lobe. VOI analysis also showed significant decreases in the parahippocampal gyrus, amygdala, and lateral temporal cortex. Previous FMZ-PET studies, using SPM for individual and group analyses, have depicted reduction of cBZR binding in the ipsilateral hippocampus in MTLE patients with unilateral hippocampal sclerosis (Koepp et al., 1996; Hammers et al., 2001) and the TLE patients without MRI abnormalities (Koepp et al., 2000; Hammers et al., 2002). Other previous studies revealed histologic, morphologic, or functional abnormalities not only in the medial part of the temporal lobe, including the hippocampus, but also in the tip and lateral cortex of the temporal lobe ipsilateral to the epileptic focus in patients with MTLE (Semah et al., 1995; Coste et al., 2002; Cendes et al., 2005). Our finding of the anterior temporal lobe abnormality extending beyond the mesial temporal structure is consistent with these previously reported findings. Satisfactory surgical outcomes were achieved in 13 of our 14 patients by means of selective amygdalohippocampectomy without anterior temporal lobectomy, suggesting that regions of the anterior temporal lobe outside the amygdala, hippocampus, and parahippocampal gyrus are not likely to be the epileptic foci of MTLE, even if they are characterized by decreased IMZ activity.

The exact role played by decreased cBZR in this region is not clear. Lack of correlation between cBZR density and neuronal density on volumetric MRI prompted Koepp et al. (1997) to conclude that atrophy with neuronal loss is not the

sole determinant of reduced cBZR binding in patients with MTLE. Decreased cBZR density is thought to reflect impaired GABAergic transmission as well as neuronal loss.

Abnormalities in extratemporal regions

In our study, significant decreases in IMZ bindings extended to extratemporal regions ipsilateral to the side of seizure onset. By VB analysis, significant decreases were detected in the insula and basal ganglia and in the medial cortices of the occipital lobe. Similarly, VOI analysis showed significant decreases in the putamen and the lateral occipital cortex. The extratemporal abnormalities we found by the two different methods shed some light on the pathology of MTLE. In line with our results, previous FMT-PET studies have reported altered extrafocal cBZR distribution in individual patients with MTLE (Hammers et al., 2001; Bouilleret et al., 2002) and neocortical partial epilepsy (Juhasz et al., 2009). Moreover, decreased extrafocal serotonin receptor density has recently been reported in individual patients with MTLE (Didelot et al., 2010). An MRI study that tracked the progression of neocortical atrophy associated with TLE revealed progressive cortical atrophy in various extratemporal lobes (Bernhardt et al., 2009). These extrafocal abnormalities likely represent seizure-induced cortical damage.

Decreased IMZ activity in the insula and the basal ganglia may be the result of direct abnormal neuronal transmission propagated from the primary epileptic focus. The insula is related to generation of the abdominal aura and epigastric discomfort (Isnard et al., 2004) experienced by patients with MTLE. The basal ganglia are thought to be involved in the generation of ictal dystonic posturing (Dupont et al., 1998) and secondarily generalized tonic-clonic seizures (Blumenfeld et al., 2009). Extratemporal glucose hypometabolism in the ipsilateral insula has been reported in patients with MTLE (Wong et al., 2010). Another group detected highly significant hypometabolism and decreased cBZR in the insular cortices of patients with MTLE (Bouilleret et al., 2002); furthermore, the insular hypometabolism did not influence outcomes after anterior temporal lobectomy. Most of our study patients experienced abdominal auras, some showed contralateral dystonic posturing, and all obtained a satisfactory outcome after surgery. Therefore, decreased IMZ activity in the insula and basal ganglia is not necessarily indicative of secondary epileptic foci.

A decrease in IMZ activity was also revealed in the ipsilateral occipital lobe by both VB and VOI analyses. Various extratemporal neocortices are reported to be abnormal or functionally impaired in patients with MTLE (Cendes et al., 2005). Several FDG-PET-based studies have shown that various neocortices, including the occipital lobe, can exist as functional deficit zones (Henry et al., 1990; Arnold et al., 1996; Wong et al., 2010). Wong et al. (2010) reported ipsilateral glucose hypometabolism in the medial and lateral occipital lobe in patients with MTLE. The occipital decrease in IMZ bindings in our study patients is consistent with this finding. A white matter associative tract connecting the temporal and occipital lobes is known as the inferior longitudinal fasciculus. A diffusion tensor imaging study showed direct connections between the temporal and occipital lobe. The temporal branches start at the parahippocampal gyrus, amygdala and lateral temporal cortex, and the occipital branches terminate at the lateral and medial occipital cortex (Catani et al., 2003). This connection, which allows propagation of abnormal epileptogenic discharges, may be affected by the occipital decrease we observed.

In conclusion, the data yielded by our VB and VOI analyses of interhemispheric IMZ activity indicate that destructive inhibitory dysfunction spreads from the mesial temporal lobe to the anterior temporal lobe and extends to basal ganglia, insula, and occipital lobe in patients with MTLE. We expect these findings, along with further individual investigations, to contribute to understanding of the pathophysiology of seizure propagation and to the diagnosis of MTLE.

Disclosure of conflicts of interest

None of the authors has any conflict of interest to disclose. We confirm that we have read the Journal's position on issues involved in ethical publication and affirm that this report is consistent with those guidelines.

Acknowledgment

This work was supported in part by a Grant-in-Aid for Scientific Research (21591869) from the Ministry of Education, Culture, Sports, Science and Technology of Japan.

References

Arnold, S., Schlaug, G., Niemann, H., Ebner, A., Luders, H., Witte, O.W., Seitz, R.J., 1996. Topography of interictal glucose hypometabolism in unilateral mesiotemporal epilepsy. Neurology 46, 1422–1430.

Aubert-Broche, B., Jannin, P., Biraben, A., Bernard, A.M., Haegelen, C., Le Jeune, F.P., Gibaud, B., 2005. Evaluation of methods to detect interhemispheric asymmetry on cerebral perfusion SPECT: application to epilepsy. J. Nucl. Med. 46, 707–713.

Beer, H.F., Blauenstein, P.A., Hasler, P.H., Delaloye, B., Riccabona, G., Bangerl, I., Hunkeler, W., Bonetti, E.P., Pieri, L., Richards, J.G., Schubiger, P.A., 1990. In vitro and in vivo evaluation of iodine-123-Ro 16-0154: a new imaging agent for SPECT investigations of benzodiazepine receptors. J. Nucl. Med. 31, 1007–1014.

Bernhardt, B.C., Worsley, K.J., Kim, H., Evans, A.C., Bernasconi, A., Bernasconi, N., 2009. Longitudinal and cross-sectional analysis of atrophy in pharmacoresistant temporal lobe epilepsy. Neurology 72, 1747–1754.

Blumenfeld, H., Varghese, G.I., Purcaro, M.J., Motelow, J.E., Enev, M., McNally, K.A., Levin, A.R., Hirsch, L.J., Tikofsky, R., Zubal, I.G., Paige, A.L., Spencer, S.S., 2009. Cortical and subcortical networks in human secondarily generalized tonic-clonic seizures. Brain 132, 999–1012.

Bouilleret, V., Dupont, S., Spelle, L., Baulac, M., Samson, Y., Semah, F., 2002. Insular cortex involvement in mesiotemporal lobe epilepsy: a positron emission tomography study. Ann. Neurol. 51, 202–208.

Brett, M., Johnsrude, I.S., Owen, A.M., 2002. The problem of functional localization in the human brain. Nat. Rev. Neurosci. 3, 243–249.

Catani, M., Jones, D.K., Donato, R., Ffytche, D.H., 2003. Occipito-temporal connections in the human brain. Brain 126, 2093–2107.

Cendes, F., Kahane, P., Brodie, M., Andermann, F., 2005. The mesiotemporal lobe epilepsy syndrome. In: Roger, J., Bureau, M., Dravet, C., Genton, P., Tassinari, C.A., Wolf, P. (Eds.), Epileptic Syndromes in Infancy, Childhood and Adolescence. John Libbey Eurotext Ltd., Montrouge, pp. 555–578.

Coste, S., Ryvlin, P., Hermier, M., Ostrowsky, K., Adeleine, P., Froment, J.C., Mauguiere, F., 2002. Temporopolar changes in temporal lobe epilepsy: a quantitative MRI-based study. Neurology 59, 855–861.

Didelot, A., Mauguiere, F., Redoute, J., Bouvard, S., Lothe, A., Reilhac, A., Hammers, A., Costes, N., Ryvlin, P., 2010. Voxel-based analysis of asymmetry index maps increases the specificity of 18F-MPPF PET abnormalities for localizing the epileptogenic zone in temporal lobe epilepsies. J. Nucl. Med. 51, 1732–1739.

Dupont, S., Semah, F., Baulac, M., Samson, Y., 1998. The underlying pathophysiology of ictal dystonia in temporal lobe epilepsy: an FDG-PET study. Neurology 51, 1289–1292.

Engel Jr., J., Van Ness, P.C., Rasmussen, T., Ojemann, L.M., 1993. Outcome with respect to epileptic seizures. In: Engel Jr., J. (Ed.), Surgical Treatment of the Epilepsies. Raven Press, New York, pp. 609–622.

Friston, K.J., Ashburner, J., Poline, J.B., Frith, C.D., Heather, J.D., Frackowiak, R.S., 1995a. Spatial registration and normalization of images. Hum. Brain Mapp. 2, 165–189.

Friston, K.J., Holmes, A.P., Worsley, K.J., Poline, J.B., Frith, C.D., Frackowiak, R.S., 1995b. Statistical parametric maps in functional imaging: a general linear approach. Hum. Brain Mapp. 2, 189–210.

Hammers, A., Koepp, M.J., Labbe, C., Brooks, D.J., Thom, M., Cunningham, V.J., Duncan, J.S., 2001. Neocortical abnormalities of [^{11}C]-flumazenil PET in mesial temporal lobe epilepsy. Neurology 56, 897–906.

Hammers, A., Koepp, M.J., Hurlemann, R., Thom, M., Richardson, M.P., Brooks, D.J., Duncan, J.S., 2002. Abnormalities of grey and white matter [^{11}C]flumazenil binding in temporal lobe epilepsy with normal MRI. Brain 125, 2257–2271.

Hammers, A., Panagoda, P., Heckemann, R.A., Kelsch, W., Turkheimer, F.E., Brooks, D.J., Duncan, J.S., Koepp, M.J., 2008. [^{11}C]Flumazenil PET in temporal lobe epilepsy: do we need an arterial input function or kinetic modeling? J. Cereb. Blood Flow Metab. 28, 207–216.

Heinzel, A., Steinke, R., Poeppel, T.D., Grosser, O., Bogerts, B., Otto, H., Northoff, G., 2008. S-ketamine and GABA-A-receptor interaction in humans: an exploratory study with I-123-iomazenil SPECT. Hum. Psychopharmacol. 23, 549–554.

Henry, T.R., Mazziotta, J.C., Engel Jr., J., Christenson, P.D., Zhang, J.X., Phelps, M.E., Kuhl, D.E., 1990. Quantifying interictal metabolic activity in human temporal lobe epilepsy. J. Cereb. Blood Flow Metab. 10, 748–757.

Hosoda, K., Kawaguchi, T., Ishii, K., Minoshima, S., Kohmura, E., 2005. Comparison of conventional region of interest and statistical mapping method in brain single-photon emission computed tomography for prediction of hyperperfusion after carotid endarterectomy. Neurosurgery 57, 32–41.

Ishii, K., Willoch, F., Minoshima, S., Drzezga, A., Ficaro, E.P., Cross, D.J., Kuhl, D.E., Schwaiger, M., 2001. Statistical brain mapping of 18F-FDG PET in Alzheimer's disease: validation of anatomic standardization for atrophied brains. J. Nucl. Med. 42, 548–557.

Isnard, J., Guenot, M., Sindou, M., Mauguiere, F., 2004. Clinical manifestations of insular lobe seizures: a stereo-electroencephalographic study. Epilepsia 45, 1079–1090.

Johnson, E.W., de Lanerolle, N.C., Kim, J.H., Sundaresan, S., Spencer, D.D., Mattson, R.H., Zoghbi, S.S., Baldwin, R.M., Hoffer, P.B., Seibyl, J.P., Innis, R.B., 1992. "Central" and "peripheral" benzodiazepine receptors: opposite changes in human epileptogenic tissue. Neurology 42, 811–815.

Juhasz, C., Asano, E., Shah, A., Chugani, D.C., Batista, C.E., Muzik, O., Sood, S., Chugani, H.T., 2009. Focal decreases of cortical GABAA receptor binding remote from the primary seizure focus: what do they indicate? Epilepsia 50, 240–250.

Kaneko, K., Sasaki, M., Morioka, T., Koga, H., Abe, K., Sawamoto, H., Ohya, N., Yoshiura, T., Mihara, F., Honda, H., 2006. Presurgical identification of epileptogenic areas in temporal lobe epilepsy by ^{123}I-iomazenil SPECT: a comparison with IMP SPECT and FDG PET. Nucl. Med. Commun. 27, 893–899.

Kim, Y.K., Lee, D.S., Lee, S.K., Kim, S.K., Chung, C.K., Chang, K.H., Choi, K.Y., Chung, J.K., Lee, M.C., 2003. Differential features of metabolic abnormalities between medial and lateral temporal lobe epilepsy: quantitative analysis of (18)F-FDG PET using SPM. J. Nucl. Med. 44, 1006–1012.

Kimura, K., Hashikawa, K., Etani, H., Uehara, A., Kozuka, T., Moriwaki, H., Isaka, Y., Matsumoto, M., Kamada, T., Moriyama, H., Tabuchi, H., 1990. A new apparatus for brain imaging: four-head rotating gamma camera single-photon emission computed tomograph. J. Nucl. Med. 31, 603–609.

Koepp, M.J., Richardson, M.P., Brooks, D.J., Poline, J.B., Van Paesschen, W., Friston, K.J., Duncan, J.S., 1996. Cerebral benzodiazepine receptors in hippocampal sclerosis. An objective in vivo analysis. Brain 119, 1677–1687.

Koepp, M.J., Richardson, M.P., Labbe, C., Brooks, D.J., Cunningham, V.J., Ashburner, J., Van Paesschen, W., Revesz, T., Duncan, J.S., 1997. ^{11}C-flumazenil PET, volumetric MRI, and quantitative pathology in mesial temporal lobe epilepsy. Neurology 49, 764–773.

Koepp, M.J., Hammers, A., Labbe, C., Woermann, F.G., Brooks, D.J., Duncan, J.S., 2000. ^{11}C-flumazenil PET in patients with refractory temporal lobe epilepsy and normal MRI. Neurology 54, 332–339.

Kugaya, A., Sanacora, G., Verhoeff, N.P., Fujita, M., Mason, G.F., Seneca, N.M., Bozkurt, A., Khan, S.A., Anand, A., Degen, K., Charney, D.S., Zoghbi, S.S., Baldwin, R.M., Seibyl, J.P., Innis, R.B., 2003. Cerebral benzodiazepine receptors in depressed patients measured with [^{123}I]iomazenil SPECT. Biol. Psychiatry 54, 792–799.

Kurokawa, K., Jibiki, I., Matsuda, H., Fukushima, T., Tsuji, S., Yamaguchi, N., Hisada, K., 1994. Comparison of benzodiazepine receptor and regional cerebral blood flow imaging of epileptiform foci in hippocampal kindled rabbits: a study with in vivo double tracer autoradiography using ^{125}I-iomazenil and 99mTc-HMPAO. Brain Res. 642, 303–310.

Minoshima, S., Koeppe, R.A., Frey, K.A., Kuhl, D.E., 1994. Anatomic standardization: linear scaling and nonlinear warping of functional brain images. J. Nucl. Med. 35, 1528–1537.

Minoshima, S., Frey, K.A., Koeppe, R.A., Foster, N.L., Kuhl, D.E., 1995. A diagnostic approach in Alzheimer's disease using three-dimensional stereotactic surface projections of fluorine-18-FDG PET. J. Nucl. Med. 36, 1238–1248.

Schubiger, P.A., Hasler, P.H., Beer-Wohlfahrt, H., Bekier, A., Oettli, R., Cordes, M., Ferstl, F., Deisenhammer, E., De Roo, M., Moser, E., Nitzsche, E., Podreka, I., Riccabona, G., Bangerl, I., Schober, O., Bartenstein, P., Van Rijk, P., Van Isselt, J.W., Van Royen, E.A., Verhoeff, N.P., Haldemann, R., Von Schulthess, G.K., 1991. Evaluation of a multicentre study with Iomazenil – a benzodiazepine receptor ligand. Nucl. Med. Commun. 12, 569–582.

Semah, F., Baulac, M., Hasboun, D., Frouin, V., Mangin, J.F., Papageorgiou, S., Leroy-Willig, A., Philippon, J., Laplane, D., Samson, Y., 1995. Is interictal temporal hypometabolism related to mesial temporal sclerosis? A positron emission tomography/magnetic resonance imaging confrontation. Epilepsia 36, 447–456.

Takada, S., Yoshimura, M., Shindo, H., Saito, K., Koizumi, K., Utsumi, H., Abe, K., 2006. New semiquantitative assessment of ^{123}I-FP-CIT by an anatomical standardization method. Ann. Nucl. Med. 20, 477–484.

Talairach, J., Tournoux, P., 1988. Co-planar Stereotaxic Atlas of the Human Brain. Thieme, New York.

Tanaka, F., Yonekura, Y., Ikeda, A., Terada, K., Mikuni, N., Nishizawa, S., Ishizu, K., Okazawa, H., Hattori, N., Shibasaki, H., Konishi, J., Onishi, Y., 1997. Presurgical identification of epileptic foci with iodine-123 iomazenil SPET: comparison with brain perfusion SPET and FDG PET. Eur. J. Nucl. Med. 24, 27–34.

Umeoka, S., Matsuda, K., Baba, K., Usui, N., Tottori, T., Terada, K., Usui, K., Nakamura, F., Inoue, Y., Fujiwara, T., Mihara, T., 2007. Usefulness of ^{123}I-iomazenil single-photon emission computed tomography in discriminating between mesial and lateral temporal lobe epilepsy in patients in whom magnetic resonance imaging demonstrates normal findings. J. Neurosurg. 107, 352–363.

Van Bogaert, P., Massager, N., Tugendhaft, P., Wikler, D., Damhaut, P., Levivier, M., Brotchi, J., Goldman, S., 2000. Statistical parametric mapping of regional glucose metabolism in mesial temporal lobe epilepsy. Neuroimage 12, 129–138.

Wong, C.H., Bleasel, A., Wen, L., Eberl, S., Byth, K., Fulham, M., Somerville, E., Mohamed, A., 2010. The topography and significance of extratemporal hypometabolism in refractory mesial temporal lobe epilepsy examined by FDG-PET. Epilepsia 51, 1365–1373.

BRAIN RESEARCH 1468 (2012) 29–37

Available online at www.sciencedirect.com

SciVerse ScienceDirect

www.elsevier.com/locate/brainres

BRAIN RESEARCH

Research Report

Neural decoding of unilateral upper limb movements using single trial MEG signals☆

Hisato Sugata[a,1], *Tetsu Goto*[a,b], *Masayuki Hirata*[a,b,*], *Takufumi Yanagisawa*[b,c], *Morris Shayne*[b], *Kojiro Matsushita*[b], *Toshiki Yoshimine*[b], *Shiro Yorifuji*[a]

[a]*Division of Functional Diagnostic Science, Osaka University Graduate School of Medicine, 1-7 Yamadaoka, Suita, Osaka, 565-0871, Japan*
[b]*Department of Neurosurgery, Osaka University Medical School, 2-2 E6 Yamadaoka, Suita, Osaka, 565-0871, Japan*
[c]*ATR Computational Neuroscience Laboratories, 2-2-2 Hikaridai, Keihannna Science City, Kyoto, 619-0288, Japan*

ARTICLE INFO

Article history:
Accepted 29 May 2012
Available online 8 June 2012

Keywords:
Brain machine interface
Magnetoencephalography
Unilateral movement
Somatotopic organization

ABSTRACT

A brain machine interface (BMI) provides the possibility of controlling such external devices as prosthetic arms for patients with severe motor dysfunction using their own brain signals. However, there have been few studies investigating the decoding accuracy for multiclasses of useful unilateral upper limb movements using non-invasive measurements. We investigated the decoding accuracy for classifying three types of unilateral upper limb movements using single-trial magnetoencephalography (MEG) signals. Neuromagnetic activities were recorded in 9 healthy subjects performing 3 types of right upper limb movements: hand grasping, pinching, and elbow flexion. A support vector machine was used to classify the single-trial MEG signals. The movement types were predicted with an average accuracy of 66±10% (chance level: 33.3%) using neuromagnetic activity during a 400-ms interval (−200 ms to 200 ms from movement onsets). To explore the time-dependency of the decoding accuracy, we also examined the time course of decoding accuracy in 50-ms sliding windows from −500 ms to 500 ms. Decoding accuracies significantly increased and peaked once before (50.1±4.9%) and twice after (58.5±7.5% and 64.4±7.6%) movement onsets in all subjects. Significant variability in the decoding features in the first peak was evident in the channels over the parietal area and in the second and third peaks in the channels over the sensorimotor area. Our results indicate that the three types of unilateral upper limb movement can be inferred with high accuracy by detecting differences in movement-related brain activity in the parietal and sensorimotor areas.

☆ Conflict of interest and source funding: None of the authors claim any conflicts of interest. Masayuki Hirata and Toshiki Yoshimine received a grant for "Brain Machine Interface Development" from the Strategic Research Program for Brain Sciences by the Ministry of Education, Culture, Sports, Science, and Technology of Japan.

* *Corresponding author at:* Department of Neurosurgery, Osaka University Medical School, 2-2 E6 Yamadaoka, Suita, Osaka, 565-0871, Japan. Fax: +81 6 6879 3659.
E-mail address: mhirata@nsurg.med.osaka-u.ac.jp (M. Hirata).
[1] Present address: Department of Neurosurgery, Osaka University Medical School, 2-2 E6 Yamadaoka, Suita, Osaka, 565-0871, Japan.

0006-8993/$ – see front matter © 2012 Elsevier B.V. All rights reserved.
doi:10.1016/j.brainres.2012.05.053

1. Introduction

A brain machine interface (BMI) offers the possibility of controlling such external devices as prosthetic arms for patients with severe motor dysfunction using their own brain signals (Hochberg et al., 2006; Yanagisawa et al., 2011). Several studies examined the validity of using brain activities to accurately control these devices (Guenther et al., 2009; Mehring et al., 2003; Nijboer et al., 2008; Rickert et al., 2005; Velliste et al., 2008; Wolpaw and McFarland, 2004), and progress in methods for measuring neural activity and neural decoding have led to increased decoding performances, even when using non-invasive methods such as electroencephalography (Bradberry et al., 2010, 2011; Das et al., 2010; Lotte et al., 2007; Presacco et al., 2011), magnetoencephalography (MEG) (Battapady et al., 2009; Bradberry et al., 2009; Georgopoulos et al., 2005; Kauhanen et al., 2006b; Waldert et al., 2008), functional magnetic resonance imaging (Lee et al., 2009; Sitaram et al., 2011), and near infrared spectroscopy (Coyle et al., 2004).

In recent years, an invasive BMI study using monkeys reported that a naturalistic unilateral upper limb movement could be reconstructed using local ensembles of primary motor cortex neurons (Vargas-Irwin et al., 2010), and another reported that a prosthetic arm could be controlled with high accuracy during unilateral upper limb movements using single-unit recording (Velliste et al., 2008). In human BMI studies, three types of unilateral upper limb movements were successfully decoded using electrocorticography (ECoG) in stroke patients by extracting the spatiotemporal information related to movements, allowing the patients to successfully control the robotic arm continuously in real time (Yanagisawa et al., 2011, 2012). To infer the movements from ECoG data, they used a support vector machine (SVM), a machine-learning method that uses discriminant hyper-planes to identify movement types.

Among the non-invasive BMI studies, there are several that examined the decoding of upper limb movements for movement directions (Waldert et al., 2008), trajectories (Contreras-Vidal et al., 2010; Georgopoulos et al., 2005; Toda et al., 2011), movement types (Buch et al., 2008; Kauhanen et al., 2006b), and hand velocity (Bradberry et al., 2009) using MEG, and Kauhanen et al. (2006a, 2006b) successfully classified three types of movements consisting of left and right or both index fingers. In addition, the decoding accuracies of binary classes of unilateral upper limb conditions, such as movement execution or rest (or movement stop), motor imagery or rest (or imagery stop), were classified (Battapady et al., 2009; Buch et al., 2008; Mellinger et al., 2007). Recently, unilateral multi-finger movements were successfully decoded, demonstrating the possibility of using a non-invasive BMI to control a prosthetic device (Quandt et al., 2012). However, to control devices such as prosthetic arms with high accuracy, it is important to use non-invasive measurements to examine the decoding accuracy of multi-classes of useful unilateral upper limb movements. In addition, better understanding of the time course of decoding accuracy over short time windows is indispensable for continuously controlling the prosthetic device as previously reported by our invasive BMI study (Yanagisawa et al., 2011).

In the present study, we examined the accuracy of decoding three kinds of unilateral upper limb movements using single trial MEG signals. The movement types were classified using an SVM extended for multiclass movements. In addition, to reveal how the decoding accuracy temporally varies in accordance with movement execution, we examined the time courses of decoding accuracy using short time windows. We also performed a univariate statistical analysis and a source analysis of the MEG signals to reveal which MEG channels contribute to classification of the three movements.

2. Results

2.1. *Decoding accuracy of movement classification*

The signal amplitudes from each MEG channel and time window during a 400-ms interval (−200 ms to 200 ms from movement onset) were used as the decoding feature for classifying unilateral upper limb movements. The individual decoding accuracy of each subject largely exceeded chance level (33.3%), and exhibited significantly high values (binomial test, $p<0.01$) (Fig. 1A). The averaged decoding accuracy of all subjects was 66.1±10.1% (mean±SD), which is approximately twice the chance level.

To examine whether classification performance was related to the time of movement onset, we investigated the time course of decoding accuracy. The decoding accuracy was calculated in 50-ms time windows (with 50%-overlaps) from −500 ms to 500 ms. Decoding accuracy in individuals tended to gradually increase before movement onset and peaked between 100 ms and 250 ms after onset (Fig. 1B). The time courses of decoding accuracy formed three peaks in all subjects: one peak before the onset of movement and two peaks after the movement (Table 1). The time course of decoding accuracy averaged over all subjects significantly exceeded chance level at 50 ms before movement onset and peaked after onset (binomial test, $p<0.01$; Fig. 1B).

Furthermore, to investigate whether movement-related activities contribute to the classification of movements, decoding accuracies were calculated from 40 MEG channels with neuromagnetic activities related to movement at −50 ms, 100 ms, and 200 ms (center channels; Fig. 2A) and these were compared with baseline decoding accuracies calculated from another 40 randomly chosen channels (peripheral channels) at the same time points. Decoding accuracies of the canter channels were significantly higher than those of the peripheral channels at −50 ms ($p<0.01$), 100 ms ($p<0.05$), and 200 ms ($p<0.05$; Mann–Whitney *U*-test; Fig. 2B).

2.2. *Variability of neuromagnetic activities among three movements*

To examine variability in the decoding features among the three movements, we analyzed the spatiotemporal patterns of F values at each of the MEG channels in 50-ms time windows (with 50% overlap) from −500 ms to 500 ms. Significantly high F values were distributed in the channels over the contralateral sensorimotor area synchronous with the second and third peaks of decoding accuracy (Fig. 3b,c). Interestingly, significant F values were also obtained prior to movement onset (−50 ms), contemporaneous with the first peak of decoding accuracy. These high

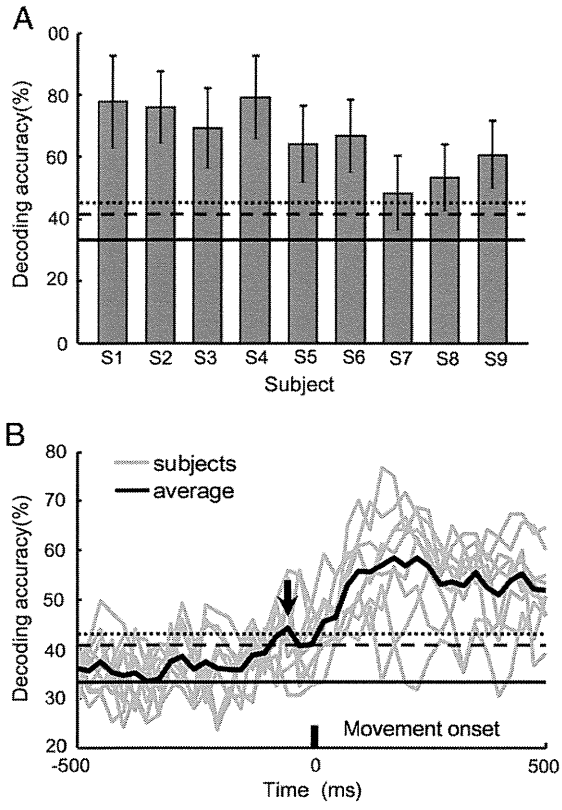

Fig. 1 – Decoding accuracy for classifying movements. (A) Individual decoding accuracies in all subjects. Three types of unilateral upper limb movements were inferred using resampled normalized amplitudes from −200 ms to 200 ms (time from movement onset) in 50-ms windows. Decoding accuracy averaged over all subjects was 66.1±10.1% (mean±SD), and individual decoding accuracies significantly exceeded chance level (33.3%, black horizontal line) in all subjects. Bars represent individual means±SD. (B) Time courses of decoding accuracy for individuals (gray curves) and the average (black curve) over all subjects. The arrow indicates the first peak in decoding accuracy at 50 ms before movement onset. The three horizontal lines indicate accuracy rates at chance level (33.3%, solid), at $p=0.05$ (dashed), and at $p=0.01$ (dotted; binomial test).

F values were located mainly in the channels over the contralateral parietal area (Fig. 3a and Supplementary movie).

The trial-averaged neuromagnetic activity in individual subjects showed large variability among the three movements in the channels with significantly high F values (Fig. 4). The differences in neuromagnetic activities were stronger for channels with high F values compared with other MEG channels. The channels with significantly high F values over the sensorimotor area showed prominent waveforms typically corresponding to movement-related cortical fields (MRCFs) (Cheyne et al., 2006; Kristeva-Feige et al., 1994) during movements.

2.3. *Cortical source localization around movements*

For each subject, we used a minimum norm estimate (MNE) to estimate 512 single-current dipoles distributed at equal distances on the cortical surface (Fig. 5). Cortical sources before movement onset were evident in the parietal area (Fig. 5A). After movement onset, cortical sources were present in the sensorimotor area during 100–150 ms from the onset (Fig. 5B). As time progressed after that, these activities decreased; but, at about 200 ms, the sensorimotor activities increased again (Fig. 5C). Intensities and distributions of the source currents in the parietal and sensorimotor areas were different among the three movements.

3. Discussion

In the present study, we classified three types of unilateral upper limb movements using MEG. The accuracy rates for decoding the movements significantly surpassed the chance level in all subjects. A time course of decoding accuracy revealed that the decoding accuracy changed relative to the movement onset, forming three peaks around the movement times in all subjects. In the first peak, before movement onset, significant variability in the neuromagnetic activities among the three movements was observed in the channels over the parietal area. In the second and third peaks, after movement onsets, significant variability was observed in the channels over the sensorimotor area. Our results indicate that multi-classes of unilateral movements can

Table 1 – Three peaks of decoding accuracy.

	First peak		Second peak		Third peak	
	Accuracy (%)	Latency (ms)	Accuracy (%)	Latency (ms)	Accuracy (%)	Latency (ms)
Sub 1	49.2	−50	69.7	125	71.7	200
Sub 2	44.7	−125	60.0	100	68.7	225
Sub 3	55.8	−50	70.0	100	76.7	150
Sub 4	57.8	−25	61.7	125	68.3	225
Sub 5	49.2	−75	60.0	100	66.7	200
Sub 6	48.3	−75	55.8	125	62.5	225
Sub 7	49.6	−50	51.4	100	52.8	150
Sub 8	54.2	−50	48.3	125	55.8	250
Sub 9	42.7	−125	50.0	125	56.7	175
Mean±SD	50.1±4.9	−69.4±32.9	58.5±7.5	113.9±12.4	64.4±7.6	200.0±33.3

SD; standard deviation.

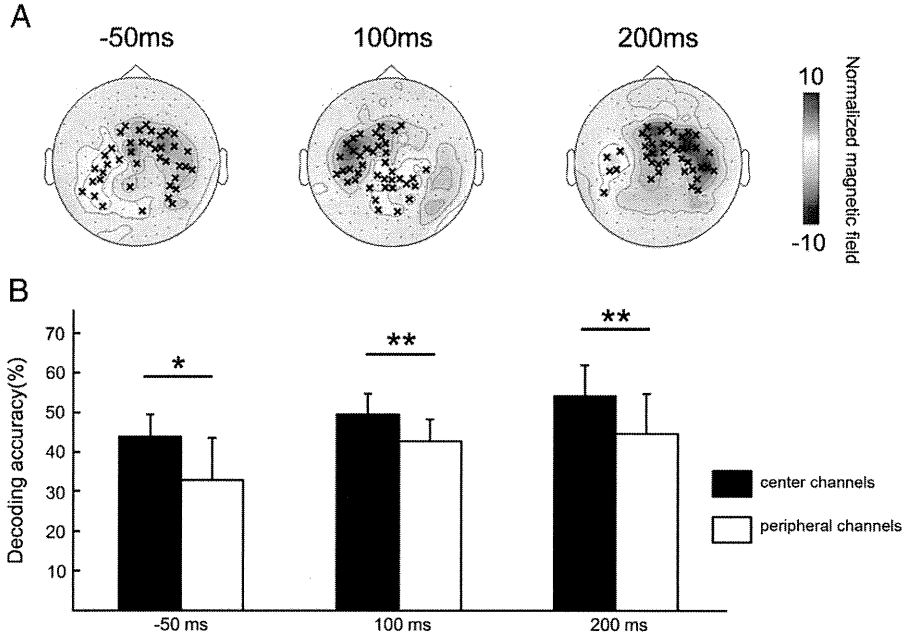

Fig. 2 – Channel definition and decoding accuracy of center channels. (A) Channel definition of center and peripheral channels. 40 MEG channels were selected from center channels (x) to examine the contribution of motor-related activities to decoding accuracy (center channels). Another 40 MEG channels were randomly selected from the remaining channels (small dots) to calculate baseline decoding accuracy (peripheral channels). (B) Mean decoding accuracies of center channels (black bars) and peripheral channels (white bars). Average decoding accuracy at the center channels was significantly higher than that at the peripheral channels at each time point (–50 ms, $p<0.01$; 100 ms, $p<0.05$, 200 ms; $p<0.05$, Mann–Whitney *U*-test).

be inferred with high decoding accuracy by detecting differences in the neuromagnetic activities related to movements in the parietal and motor-related areas.

One assumes that it is more difficult to classify unilateral upper limb movements than right and left upper limb movements, due to the close activation of unilateral brain regions. But, while there have been many studies that classified bilateral upper limb movements or binary conditions of unilateral upper limb movements by MEG (Battapady et al., 2009; Buch et al., 2008; Kauhanen et al., 2006a, 2006b; Liao et al., 2007; Mellinger et al., 2007), there have been few studies focusing on the classification of unilateral upper limb movements (Quandt et al., 2012; Waldert et al., 2009). Recently, Toda et al. (2011) succeeded in reconstructing two-dimensional trajectories of the right index fingertip from cortical currents using a hierarchical Bayesian method.

In the present study, we classified unilateral upper limb movements from the amplitude of MEG signals. To distinguish unilateral upper limb movements, we used the averaged normalized amplitudes of MEG signals as a decoding feature. This feature consists mainly of the low frequency components of the

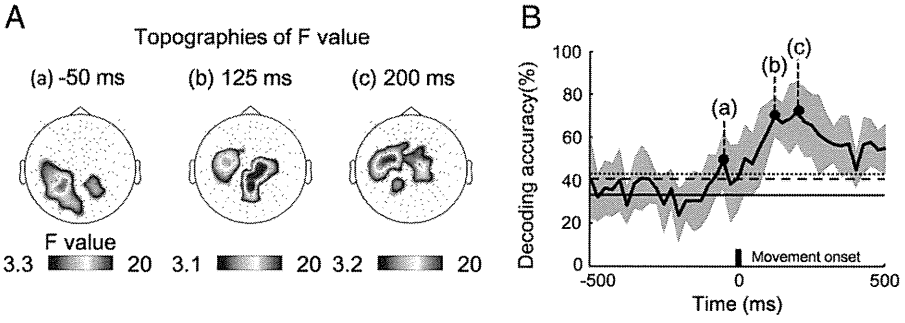

Fig. 3 – Topographies of F values for the variability of decoding features (averaged normalized amplitudes) at individual MEG channels ($p<0.05$, ANOVA) (A) and time course of decoding accuracy in one subject (B). Significant F values were observed in signals from the channels over the parietal area during the first peak of decoding accuracy (a) and over the sensorimotor area during the second and third peaks (b, c). Color bars show ranges of significant F values ($p<0.05$, ANOVA). Shaded area in (B) indicates standard deviation and the three horizontal lines indicate chance level (33.3%, solid) and significant levels at $p=0.05$ (dashed) and $p=0.01$ (dotted; binomial test).

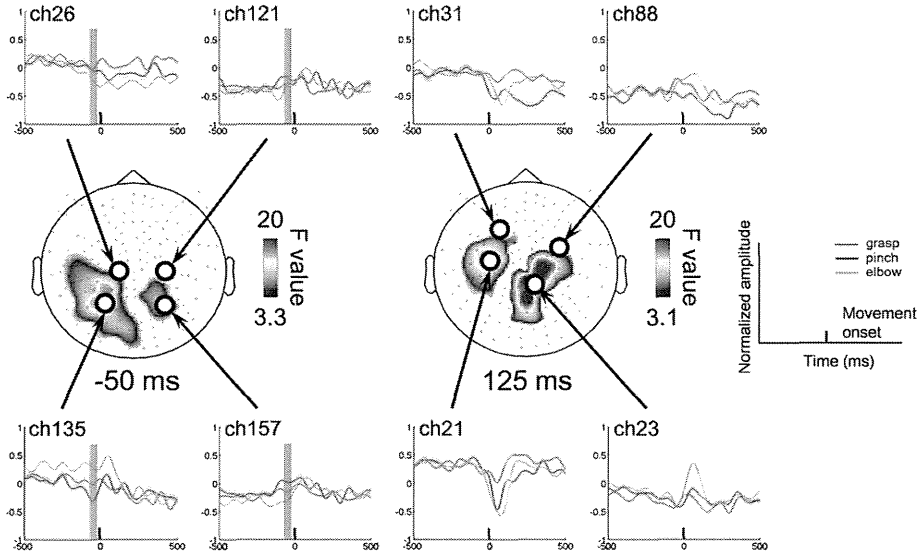

Fig. 4 – The trial-averaged neuromagnetic activity in selected channels of one subject. The curves in the upper and lower rows depict the trial-averaged neuromagnetic activities (shadow, standard error) in each movement type: blue: hand grasping, red: pinching, green: elbow flexion. Shaded vertical red and yellow bands indicate the time-windows of the topography maps of the F values. The topography maps in the middle row depict the distributions of F values computed from all channels; the circles the locations of the selected channels shown above and below. The color bars show a range of significant F values ($p<0.05$, ANOVA).

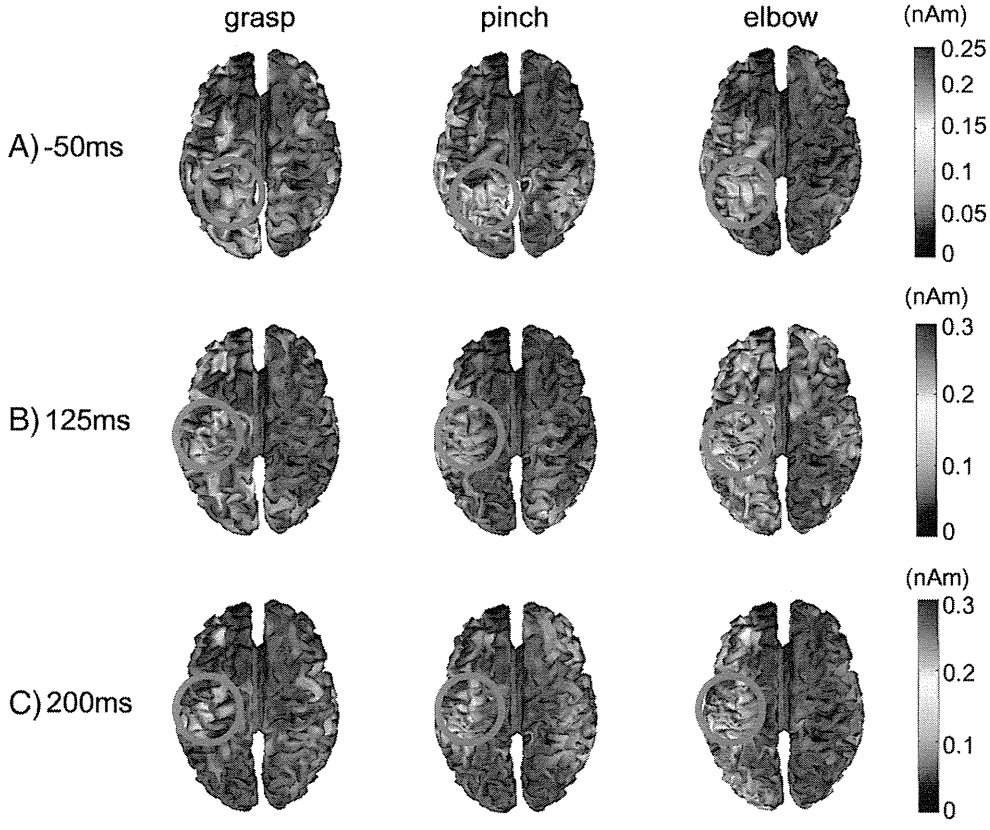

Fig. 5 – Cortical sources before (−50 ms) and after (125 ms and 200 ms) movement onset in one subject. Cortical sources were estimated using the minimum norm estimate. (A) Before movements, current sources were present around the parietal area during each movement. (B,C) After movement onset, current sources were observed around the sensorimotor area during 100–200 ms. The intensity and distribution patterns of current sources differed depending on movement type (red circles).

signals extracted by averaging within sliding time windows. The low frequency component of the signals is reported to be suitable for decoding movement trajectories (Pistohl et al., 2008; Schalk et al., 2007) and movement types (Yanagisawa et al., 2009) using invasive measurements, and movement directions (Waldert et al., 2008) using non-invasive measurements. Bradberry et al. (2009) also showed that the fluctuations in the amplitude of low-frequency MEG signals carry enough information about hand and arm movement for decoding of movement kinematics. Given that low frequency components of the signals have higher signal-to-noise ratios than high frequency components, the decoding feature used in this study may have been suited for classifying the unilateral upper limb movements with single trial MEG signals, even though MEG is inferior to invasive cortical recordings with respect to the sensitivity in weak signals in the high frequency band.

We also examined the time course of decoding accuracy, and demonstrated three peaks of decoding accuracy around the time of movement onset in all subjects. Interestingly, the first peak occurred 50 ms before movement onset. In general, it is known that brain activation related to movement, such as movement preparation and movement execution, occurs in several brain regions (Andersen and Cui, 2009; Cheyne et al., 2006; Jeannerod, 2001). For instance, a motor magnetic field (MF) recorded in channels over the motor area just before movement is an early component of the MRCFs and reflects the final cortico-spinal motor outflow from the primary motor area (Kristeva et al., 1991; Kristeva-Feige et al., 1997). In addition, conscious action plans and predictive control of movements takes place in the parietal area (Desmurget and Sirigu, 2009; Desmurget et al., 2009; Haggard, 2005; Sirigu et al., 2004). This area is also thought to encode different kinds of movement associated with different body parts (Andersen and Buneo, 2002; Kalaska et al., 1997). In our study, decoding accuracy calculated from center channels including the parietal area was significantly higher than that of baseline accuracy calculated from peripheral channels at 50 ms before movement. Furthermore, significantly high F values reflecting differences in the decoding features in each channel were evident in the channels over the parietal area during the first peak of decoding accuracy. Cortical sources were also present over the parietal area in all subjects, but intensities and distributions of current sources were different among the movements. These results indicate that differences in brain activity occurring before movements were detected by MEG channels over the parietal area as a summation of several brain activities related to movement preparation and movement execution.

During the second and third peaks of decoding accuracy, the spatial distribution of significantly high F values indicated two adjacent clusters of channels over the sensorimotor area. Corresponding to the latencies of these peaks, current sources were also present in the sensorimotor area for each movement. Furthermore, decoding accuracy calculated from center channels including the sensorimotor area was significantly higher than the baseline accuracy calculated from other peripheral channels after movement onset. In these center channels, clear MRCFs were observed. Generators of MRCFs are known to be located at the anterior and posterior walls of the central sulcus (Cheyne et al., 2006; Kristeva-Feige et al., 1997), and to exhibit different spatiotemporal patterns during different movements (Kristeva-Feige et al., 1994). A study using ECoG reported that brain signals from the anterior wall of the central sulcus exhibited more variability among three kinds of unilateral upper limb movements than those of the precentral gyrus (Yanagisawa et al., 2009), indicating that much information related to the somatotopic organization of movement types is located within the central sulcus. Thus, our results suggest that somatotopic information within the central sulcus related to movement could be measured by single trial MEG signals and decoded with high accuracy.

We achieved significantly high decoding accuracy using neuromagnetic activities consisting of low frequency components as a decoding feature, and demonstrated the relationship between fluctuation of decoding accuracies and neurophysiological activities. However, it appears that the decoding accuracies in our study were not as high as those of recent studies using other classification methods (Quandt et al., 2012; Waldert et al., 2008). Recently, Toda et al. (2011) precisely reconstructed the two-dimensional movement trajectories of unilateral upper limbs using estimated MEG source currents. They obtained high reconstruction accuracies by estimating the source currents using a hierarchical Bayesian method that solved an inverse problem by incorporating functional magnetic resonance imaging activity as a hierarchical prior (Sato et al., 2004; Yoshioka et al., 2008). Hence, by combining our method with these source current estimation methods, we may be able to further improve the classification of unilateral movements. Event-related high frequency oscillations have also been detected by MEG (Cheyne et al., 2008; Guggisberg et al., 2008) in recent studies. High frequency oscillations had greater somatotopic organization over the sensorimotor areas and tended to be more time-locked to movement onsets compared with lower frequency components (Crone et al., 1998). In the future, we also need to demonstrate whether a large variety of unilateral upper limb movement can also be classified using high frequency components as a decoding feature. Furthermore, for the purpose of motor restoration, it is also important to investigate tasks without physical movements, such as motor imagery and motor attempts, tasks we intend to focus on next. When we investigate the decoding of motor imagery, it will be important to consider the relationship between motor execution and motor imagery, because neural networks for these two partially overlap. Moreover, brain regions related to movement, such as the primary motor area and the parietal area, are similarly activated during both conditions (Gerardin et al., 2000; Jeannerod, 2001).

4. Conclusions

We examined the feasibility of classifying unilateral upper limb movements using MEG. Decoding accuracy largely exceeded chance level before and after movements and exhibited three time-related peaks. During these peaks, significant variabilities in the decoding feature were observed over the parietal and sensorimotor areas. Somatotopic organization related to movements may be measureable by single trial MEG signals, and can be utilized for classifying movement types. Further investigation of the classification of a large variety of unilateral movements in other body parts is needed to demonstrate the feasibility of a MEG-based BMI.

5. Experimental procedure

5.1. Subjects

Nine healthy volunteers participated in the study (4 males and 5 females; mean age 32.8 years, SD 14.2, range 21–59 years) after providing informed, written consent. All subjects were confirmed to be right-handed using the Edinburgh Handedness Inventory (all subjects had a score of 100), had no history of neurological or psychiatric diseases, and had normal vision. The protocol of this study was approved by the ethics committee of Osaka University Hospital.

5.2. Task

The experimental paradigm is shown in Fig. 6. An epoch started with 4 s in the resting state and visual presentation of a black fixation cross. Then, a Japanese word representing one of the three movements (grasping, pinching, and elbow flexion) was presented to instruct the subject which movement to perform after the execution cue. Each of the three movements was performed 60 times, and the movement in any given epoch was selected randomly.

5.3. Measurements and preprocessing

Neuromagnetic activities were recorded in a magnetically shielded room using a 160-channel whole-head MEG system equipped with coaxial type gradiometers (MEG vision NEO, Yokogawa Electric Corporation, Kanazawa, Japan). The subject lay on a bed in the supine position with their head centered. The head position was measured before and after recording using five coils placed on the face (the external meatus of each ear and three points on the forehead). Visual stimuli were displayed on a projection screen 325 mm from the subject's eyes using a visual presentation system (Presentation, Neurobehavioral Systems, Albany, CA) and a liquid crystal projector (LVP-HC6800, Mitsubishi Electric, Tokyo, Japan). Data were sampled at a rate of 1000 Hz with an online low-pass filter at 200 Hz. After data acquisition, a notch filter at 60 Hz was applied to eliminate the AC line noise. To reduce contamination from muscle activities and eye movements, we instructed the subjects to rest their elbows on a cushion, to avoid shoulder movements, and to watch the center of the display without ocular movements and blinking. We also recorded electromyograms of the flexor pollicis brevis, flexor digitorum superficialis, and biceps brachii muscles.

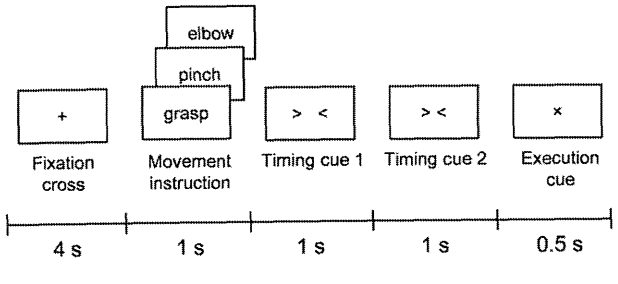

Fig. 6 – Experimental paradigm. An epoch began with a 4-s resting phase and visual presentation of a black fixation cross. A Japanese word representing one of three movements was then presented for 1 s to instruct the subject which movement to perform after the execution cue. Two 1-s timing cues were presented before the execution cue. Each of the three movements was performed 60 times.

Each movement-onset was determined by an initial rise of the most responsive electromyogram waveform; this onset time was defined as 0 ms and all time windows are in reference to this onset time. Epochs from −4000 ms to 2000 ms were analyzed. The baseline was set from −4000 ms to −3000 ms, when the subject was in the resting state. Data from each epoch were normalized by subtracting the mean and dividing by the SD of the baseline values. The normalized amplitudes of each MEG channel from −200 ms to 200 ms were then resampled over an average 100-ms time window, sliding by 50 ms. The averaged normalized amplitudes were used as a feature to classify movements.

To determine whether classification performance depends on the time from movement onset, we examined short time frames of MEG signals from −500 ms to 500 ms. The normalized signals were divided into 50-ms time windows with 50% overlap, and movements were classified for each of the 50-ms time windows.

5.4. Decoding accuracy of classifying three movements

To examine decoding accuracy, we used an SVM, operating on the Matlab 2008a software (Mathworks, Natwick, MA) that was extended to discriminate a multiclass of movements (Kamitani and Tong, 2005). The decoding accuracies were evaluated using 10-fold cross-validation. Each dataset was divided into ten parts, the classifiers were determined from 90% of the dataset (training set) and tested on the remaining 10% so that the testing dataset was independent from the training dataset each time. This procedure was then repeated ten times. The averaged percent correct over all runs was used as a measure of decoder performance. The binomial test was performed to confirm that the decoding performance significantly exceeded chance levels.

We also investigated whether movement-related neuromagnetic activities contribute to the decoding accuracy before and after movement onset. A template of the topographic pattern related to movement was created from trial-averaged neuromagnetic activity, which was calculated from all three movements in all subjects for each MEG channel at −50 ms, 100 ms, and 200 ms (time from movement onset). Then, 40 MEG channels with neuromagnetic activities related to movements at −50 ms, 100 ms, and 200 ms were selected from center channels located over the sensorimotor and parietal areas (center channels; Fig. 2A). Decoding accuracies were calculated at each time point using averaged neuromagnetic activities (±25 ms from each time point) in only the center channels. Baseline decoding accuracies were also calculated at same time points using 40 peripheral channels (peripheral channels) that were randomly selected from the remaining channels. Then, the two decoding accuracies at each time point were statistically compared by the Mann–Whitney U-test.

5.5. Statistical analysis

A one-way analysis of variance (ANOVA) was performed across each of the 50-ms time windows with 50%-overlap from −500 ms

to 500 ms to reveal the spatiotemporal differences in the magnetic fields among the three movements. Significant F values in all MEG channels were calculated using the same parameters used for calculating the time course of the decoding accuracy. The topographies of the F values were delineated on a map of MEG channels to determine which channels exhibited significant differences in neuromagnetic activities among movements.

5.6. *Cortical source localization*

To visualize the cortical activities during each of the three types of unilateral upper-limb-movements, cortical sources of the MEG signals were estimated using a minimum norm estimate (MNE) (Hamalainen and Ilmoniemi, 1994) from MRI-constrained neuromagnetic fields (Litvak et al., 2011) with SPM8 (University College of London, London, U.K.). Based on a single-shell spherical head model, the MNE calculated (with 2 cm spatial resolution) cortical electrical-currents of 512 dipolar sources evenly distributed over the brain model from the averaged neuromagnetic fields. We estimated brain activities between −500 ms and 500 ms from the movement onset.

Supplementary data to this article can be found online at http://dx.doi.org/10.1016/j.brainres.2012.05.053.

Acknowledgments

This work was supported in part by a grant to T Yoshimine for "Brain Machine Interface Development" from the Strategic Research Program for Brain Sciences funded by the Ministry of Education, Culture, Sports, Science, and Technology of Japan, and by Health Labour Sciences Research Grant (23100101) to M Hirata funded by the Ministry of Health Labour and Welfare of Japan.

REFERENCES

Andersen, R.A., Buneo, C.A., 2002. Intentional maps in posterior parietal cortex. Annu. Rev. Neurosci. 25, 189–220.

Andersen, R.A., Cui, H., 2009. Intention, action planning, and decision making in parietal–frontal circuits. Neuron 63, 568–583.

Battapady, H., Lin, P., Holroyd, T., Hallett, M., Chen, X., Fei, D.Y., Bai, O., 2009. Spatial detection of multiple movement intentions from SAM-filtered single-trial MEG signals. Clin. Neurophysiol. 120, 1978–1987.

Bradberry, T.J., Rong, F., Contreras-Vidal, J.L., 2009. Decoding center-out hand velocity from MEG signals during visuomotor adaptation. NeuroImage 47, 1691–1700.

Bradberry, T.J., Gentili, R.J., Contreras-Vidal, J.L., 2010. Reconstructing three-dimensional hand movements from noninvasive electroencephalographic signals. J. Neurosci. 30, 3432–3437.

Bradberry, T.J., Gentili, R.J., Contreras-Vidal, J.L., 2011. Fast attainment of computer cursor control with noninvasively acquired brain signals. J .Neural. Eng. 8, 036010.

Buch, E., Weber, C., Cohen, L.G., Braun, C., Dimyan, M.A., Ard, T., Mellinger, J., Caria, A., Soekadar, S., Fourkas, A., Birbaumer, N., 2008. Think to move: a neuromagnetic brain–computer interface (BCI) system for chronic stroke. Stroke 39, 910–917.

Cheyne, D., Bakhtazad, L., Gaetz, W., 2006. Spatiotemporal mapping of cortical activity accompanying voluntary movements using an event-related beamforming approach. Hum. Brain Mapp. 27, 213–229.

Cheyne, D., Bells, S., Ferrari, P., Gaetz, W., Bostan, A.C., 2008. Self-paced movements induce high-frequency gamma oscillations in primary motor cortex. NeuroImage 42, 332–342.

Contreras-Vidal, J.L., Bradberry, T.J., Agashe, H., 2010. Movement decoding from noninvasive neural signals. Conf. Proc. IEEE Eng. Med. Biol. Soc. 2010, 2825–2828.

Coyle, S., Ward, T., Markham, C., McDarby, G., 2004. On the suitability of near-infrared (NIR) systems for next-generation brain–computer interfaces. Physiol. Meas. 25, 815–822.

Crone, N.E., Miglioretti, D.L., Gordon, B., Lesser, R.P., 1998. Functional mapping of human sensorimotor cortex with electrocorticographic spectral analysis. II. Event-related synchronization in the gamma band. Brain 121 (Pt 12), 2301–2315.

Das, K., Giesbrecht, B., Eckstein, M.P., 2010. Predicting variations of perceptual performance across individuals from neural activity using pattern classifiers. NeuroImage 51, 1425–1437.

Desmurget, M., Sirigu, A., 2009. A parietal–premotor network for movement intention and motor awareness. Trends Cogn. Sci. 13, 411–419.

Desmurget, M., Reilly, K.T., Richard, N., Szathmari, A., Mottolese, C., Sirigu, A., 2009. Movement intention after parietal cortex stimulation in humans. Science 324, 811–813.

Georgopoulos, A.P., Langheim, F.J., Leuthold, A.C., Merkle, A.N., 2005. Magnetoencephalographic signals predict movement trajectory in space. Exp. Brain Res. 167, 132–135.

Gerardin, E., Sirigu, A., Lehericy, S., Poline, J.B., Gaymard, B., Marsault, C., Agid, Y., Le Bihan, D., 2000. Partially overlapping neural networks for real and imagined hand movements. Cereb. Cortex. 10, 1093–1104.

Guenther, F.H., Brumberg, J.S., Wright, E.J., Nieto-Castanon, A., Tourville, J.A., Panko, M., Law, R., Siebert, S.A., Bartels, J.L., Andreasen, D.S., Ehirim, P., Mao, H., Kennedy, P.R., 2009. A wireless brain–machine interface for real-time speech synthesis. PLoS One 4, e8218.

Guggisberg, A.G., Dalal, S.S., Findlay, A.M., Nagarajan, S.S., 2008. High-frequency oscillations in distributed neural networks reveal the dynamics of human decision making. Front. Hum. Neurosci. 1.

Haggard, P., 2005. Conscious intention and motor cognition. Trends Cogn. Sci. 9, 290–295.

Hamalainen, M.S., Ilmoniemi, R.J., 1994. Interpreting magnetic fields of the brain: minimum norm estimates. Med. Biol. Eng. Comput. 32, 35–42.

Hochberg, L.R., Serruya, M.D., Friehs, G.M., Mukand, J.A., Saleh, M., Caplan, A.H., Branner, A., Chen, D., Penn, R.D., Donoghue, J.P., 2006. Neuronal ensemble control of prosthetic devices by a human with tetraplegia. Nature 442, 164–171.

Jeannerod, M., 2001. Neural simulation of action: a unifying mechanism for motor cognition. NeuroImage 14, S103–S109.

Kalaska, J.F., Scott, S.H., Cisek, P., Sergio, L.E., 1997. Cortical control of reaching movements. Curr. Opin. Neurobiol. 7, 849–859.

Kamitani, Y., Tong, F., 2005. Decoding the visual and subjective contents of the human brain. Nat. Neurosci. 8, 679–685.

Kauhanen, L., Nykopp, T., Lehtonen, J., Jylanki, P., Heikkonen, J., Rantanen, P., Alaranta, H., Sams, M., 2006a. EEG and MEG brain–computer interface for tetraplegic patients. IEEE Trans. Neural Syst. Rehabil. Eng. 14, 190–193.

Kauhanen, L., Nykopp, T., Sams, M., 2006b. Classification of single MEG trials related to left and right index finger movements. Clin. Neurophysiol. 117, 430–439.

Kristeva, R., Cheyne, D., Deecke, L., 1991. Neuromagnetic fields accompanying unilateral and bilateral voluntary movements: topography and analysis of cortical sources. Electroencephalogr. Clin. Neurophysiol. 81, 284–298.

Kristeva-Feige, R., Walter, H., Lutkenhoner, B., Hampson, S., Ross, B., Knorr, U., Steinmetz, H., Cheyne, D., 1994. A neuromagnetic